Department of Physics and Astronomy
University of Heidelberg

Bachelor Thesis in Physics
submitted by

Edgar Cristopher Cortés García

born in Ciudad de México (México)

2018

Limitations of a linear transfer map method for finding matched distributions in high intensity cyclotrons

This Bachelor Thesis has been carried out by Edgar Cristopher Cortés García at the
Paul Scherrer Institute in Villigen, Switzerland
under the supervision of
Prof. André Schöning and Ph.D. Andreas Adelmann

UNIVERSITÄT
HEIDELBERG
ZUKUNFT
SEIT 1386

PAUL SCHERRER INSTITUT

Limitations of a linear transfer map method for finding matched distributions in high intensity cyclotrons

Bachelor Thesis

in Physics

Department of Physics and Astronomy

Heidelberg University

written by

Edgar Cristopher Cortés García

supervised by

Dr. A. Adelmann
Prof. A. Schöning

October 2018

Abstract

The very well known theory of linear ion optics offers a simple method to compute matched distributions for a given lattice. For a system where a strong space charge effect has to be taken into consideration a numerical method to find such distributions was suggested in [1], supposing a linear space charge and elliptical symmetry is present on the system. It's implementation in the OPAL framework can be found on [2]. In this thesis the matched distributions are computed for the high intensity cyclotrons at PSI with real field maps. Then, normal distributions are generated and tracked with a PIC algorithm, where also non-linear terms can be modeled. The results give an insight on the machine characteristics, as well as the limitations of the truncation of the linear theory, which compromises the symplectic condition, and how this affects the matching.

Zusammenfassung

Die gut bekannte lineare Ionenoptiktheorie bietet eine einfache Methode an, um so gennante 'Eigenverteilungen'(eng. matched Distributions) für ein gegebenes ionenoptisches System zu berechnen. Für ein System, bei welchem ein starker Raumladungseffekt eine große Rolle spielt, wurde eine numerische Methode in [1] beschrieben, um solche Verteilungen zu finden, angenommen elliptische Symmetrie und ein linearer Raumladungseffekt vorhanden sind. Dieses Verfahren und die Implementation in OPAL werden in [2] beschrieben. In dieser Bachelorarbeit werden diese Verteilungen in den Hochintensitäts-Zyklotronen am PSI mit reellen magnetischen Feldern gesucht. Danach werden normale Verteilungen mit einem PIC Algorithmus verfolgt, wobei auch nicht-lineare Terme berücksichtigt werden können. Die Ergebnisse lassen sowohl wichtige Eigenschaften der Zyklotronen erkennen als auch die Begrenzungen und Auswirkungen der linearen Näherung, wodurch die symplektische Bedingung verletzt wird.

Contents

List of Figures

Chapter 1

Theoretical background

1.1 Introduction

In high intensity cyclotrons, as well as in other particle accelerators, it is of uttermost importance ensuring the stability and quality of the beam during injection, transport, acceleration and extraction processes. Consequently the computation and engineering of a proper Hamiltonian within the system has to be studied intensively to understand the relevant processes arising in the accelerator. In a system where a strong space charge effect is present, due to the high amount of charged particles, the Coulomb repulsion unstabilizes the bunch leading to particle loss, bad quality of the bunch, among others. Studying the possible stable configurations of coasting bunches (no energy gain) is the first step to later study such bunches considering acceleration.

In order to better study these phenomena high performance computing recently showed to be a suitable tool for optimization before and/or after the construction of any experimental setup. Simulation methods have been referred as the third pillar of science (together with theory and experimentation). This thesis describes a possible way of computing a stable coasting bunch and then assesses its limitations by comparing the results with a high fidelity model. All the simulations were made in the Object-oriented Particle Accelerator Library (OPAL) framework. OPAL is an open source tool for charged-particle optics in large accelerator structures and beam lines. It includes 3D space charge effects, particle matter interaction and multi-objective optimization.

We compute the matched distributions for the two high intensity cyclotrons at PSI, where we take into consideration following assumptions:

- There is no energy loss or gain in the system. (coasting bunch)
- The bunch moves in a closed orbit in the cyclotron. (equilibrium orbit)
- No particle get lost.

This chapter describes the two approaches, which are mostly used by the particle accelerator community to track particles. The Particle in Cell (PIC) and the transfer matrix methods are well centered around the Hamilton formalism but differ on accuracy and computational power needed to perform a simulation. It is intended to give details on the underlying physical theories and methods, which were used to model the system and not the implementation details on the OPAL framework. For more details about the OPAL framework refer to [3]. Furthermore the concepts of a matched distribution are reviewed together with the relevant concepts in the underlying model.

In the following chapters the studied high intensity cyclotrons at PSI are described with the results of the simulations. In the last chapter the results are analyzed and discussed.

1.1.1 Coordinate system

The coordinate system by itself is constraint to the submanifold of the spatial dimensions given by the particle accelerator. For this end, the preferred coordinate system used by the community is given around the nominal (or reference) orbit s. The coordinate system is given by the deviations from the reference orbit s and the deviation to the nominal momentum at s

$$\vec{x} = \begin{pmatrix} x(s) \\ x'(s) \\ z(s) \\ z'(s) \\ l(s) \\ \delta(s) \end{pmatrix}, \tag{1.1}$$

with

$$x = x_k - x_0, \qquad z = z_k - z_0, \qquad l = l_k - l_0, \tag{1.2}$$

$$x' = \frac{dx}{ds}, \qquad z' = \frac{dz}{ds}, \qquad \delta = \frac{p - p_0}{p_0}. \tag{1.3}$$

Here the subindex "0" denotes the reference value at s and the subindex k denotes the actual position in that direction. The cyclotron community also reserves the z-coordinate to be the one which points in direction of the external magnetic field and its normally the vertical direction. The x-coordinate is reserved for the horizontal direction and in the cyclotron community, it is mostly the radial direction from the cylindrical coordinates.

Lastly, the last coordinate is identified as l (like in [4]), it points in the longitudinal direction of the motion, and is equivalent to the direction in which the normal vector $\vec{e}_\theta$ points at in cylindrical coordinates, namely, perpendicular to x and z (in a right handed system). In the literature one might find it is commonly referred also as the y-coordinate. The coordinates x' and z' contain implicitly the moment deviation in their planes respectively and the coordinate δ is the total relative moment deviation. The following figure shows the accompaning coordinate system often also known as Frenet-Serret coordinates.

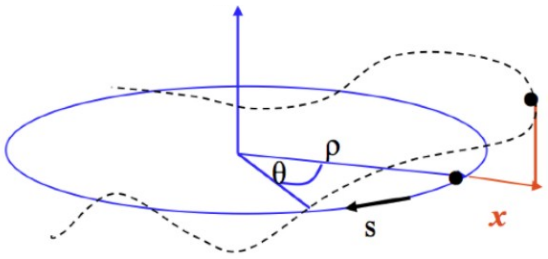

Figure 1.1: Coordinate system. Source: [18]

The blue arrow points in the direction of z. The symbol ρ represents the nominal radius in laboratory system.

1.1.2 Classical cyclotron

The cyclotron concept was first proposed by E. O. Lawrence and further developed at Berkeley in 1932. Cyclotrons are circular particle accelerators and are not well suited to reach high energies, as good as synchrotrons, but they can deliver and accelerate continuously bunches of particles. The "classic" cyclotron is based on the idea that the rotational frequency of a charged particle in a constant external magnetic field is also constant, i.e.

$$\omega_0 = \frac{Q}{\gamma m} B_0 = constant, \tag{1.4}$$

where ω_0 is the rotational frequency, also called cyclotron frequency, γ is the Lorentz factor, m is the mass of the particle, Q is the charge of the particle and B_0 is the magnetic field. The acceleration scheme is given by two hollow "D" electrodes, which work as a high frequency (HF) resonator. An illustration of the concept can be seen in Fig. 1.2.

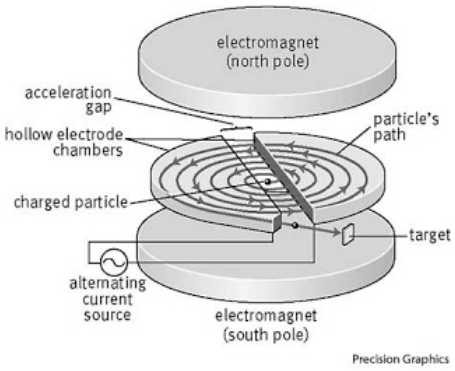

Figure 1.2: Schematics of a classic cyclotron. Source:[19]

Eq. 1.4 holds as long as $\gamma \approx 1$. The frequency at the electrodes is given by

$$\nu_{HF} = \frac{N_h}{2\pi} \frac{qB_0}{m}, \tag{1.5}$$

in other words, the frequency of the accelerating voltage must be equal to $\frac{\omega_0}{2\pi}$ or an integer multiple of it, often called the harmonic number N_h.

1.1.3 Isochroncyclotron

For a more relativistic case $B \propto \gamma$ should hold to fulfill the isochronicity ($\omega = const$) of the acceleration. The following simplified cyclotron model together with some quantities for the description of the system can be found in [1]. First a cyclotron length unit a is defined as

$$a = \frac{c}{\omega_0}, \tag{1.6}$$

where c is the speed of light and ω_0 is given by Eq. 1.4 with $\gamma = 1$ and B_0 the average magnetic field. Since the rotation velocity is given by $v = \omega_0 \rho$ it follows that $\beta = v/c = \rho/a$. From this

we get

$$\gamma(\rho) = \frac{1}{\sqrt{1-(\frac{\rho}{a})^2}}. \tag{1.7}$$

The magnetic field as function of the radius should the increase as

$$B(\rho) = B_0\gamma(\rho) = \frac{B_0}{\sqrt{1-(\frac{\rho}{a})^2}}. \tag{1.8}$$

The field index n given by

$$n = \frac{\rho}{B}\frac{dB}{d\rho}. \tag{1.9}$$

and is an important quantity of the system(see Sec 1.3.1). The key concept of a isochron-cyclotron is the capability of creating a magnetic field, which grows as described by Eq. 1.8, so that the rotational frequency stays constant. The HF-Resonators can be then driven with the frequency described in Eq. 1.5. At PSI the magnetic field of the Ring Cyclotron, which accelerates protons from 72MeV up to 590MeV is produced by sector magnets (Figure 1.3).

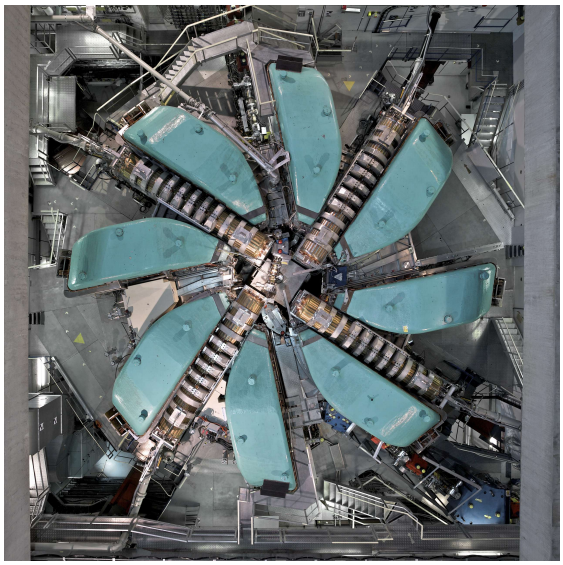

Figure 1.3: Ring cyclotron at PSI. Source: [20]

The Ring is a isochron-sector-cyclotron and produces one of the most powerful proton beams in the world, capable of delivering ∼2.2mA and a power of ∼1.3MW.

1.1.4 σ - Matrix

In particle accelerators, the current yields from a couple of nA to hundreds of mA. At PSI the number of protons in a bunch is around $N \approx 10^8$. A practical way to describe a bunch is by its so called σ-matrix. Given a collection of particles in a bunch we can compute the matrix

$$\sigma_{ij} = \langle (x_i - \langle x_j \rangle)^2 \rangle, \qquad x_i \in [x, x', z, z', l, \delta], \tag{1.10}$$

where $\langle \cdot \rangle$ represents the mean defined as $\langle x_i \rangle = \frac{1}{N} \sum_{n=1}^{N} x_{i,n}$. In our system the bunches should be well centered around the reference orbit s, hence the matrix has the form

$$\sigma = \begin{pmatrix} \langle x^2 \rangle & \langle xx' \rangle & \langle xz \rangle & \langle xz' \rangle & \langle xl \rangle & \langle x\delta \rangle \\ \langle x'x \rangle & \langle x'^2 \rangle & \langle x'z \rangle & \langle x'z' \rangle & \langle x'l \rangle & \langle x'\delta \rangle \\ \langle zx \rangle & \langle zx' \rangle & \langle z^2 \rangle & \langle zz' \rangle & \langle zl \rangle & \langle z\delta \rangle \\ \langle z'x \rangle & \langle x'z' \rangle & \langle z'z \rangle & \langle z'^2 \rangle & \langle z'l \rangle & \langle z'\delta \rangle \\ \langle lx \rangle & \langle lx' \rangle & \langle lz \rangle & \langle lz' \rangle & \langle l^2 \rangle & \langle l\delta \rangle \\ \langle \delta x \rangle & \langle \delta x' \rangle & \langle \delta z \rangle & \langle \delta z' \rangle & \langle \delta l \rangle & \langle \delta^2 \rangle \end{pmatrix}. \tag{1.11}$$

The bunch sizes are then given by the standard deviation $\sigma_i = \sqrt{\langle x_i^2 \rangle}$. From the assumption of midplane and azimuthal symmetrie, it follows that the vertical direction should be independent from the other two. This means for the σ-matrix

$$\sigma = \begin{pmatrix} \langle x^2 \rangle & \langle xx' \rangle & 0 & 0 & \langle xl \rangle & \langle x\delta \rangle \\ \langle x'x \rangle & \langle x'^2 \rangle & 0 & 0 & \langle x'l \rangle & \langle x'\delta \rangle \\ 0 & 0 & \langle z^2 \rangle & \langle zz' \rangle & 0 & 0 \\ 0 & 0 & \langle z'z \rangle & \langle z'^2 \rangle & 0 & 0 \\ \langle lx \rangle & \langle lx' \rangle & 0 & 0 & \langle l^2 \rangle & \langle l\delta \rangle \\ \langle \delta x \rangle & \langle \delta x' \rangle & 0 & 0 & \langle \delta l \rangle & \langle \delta^2 \rangle \end{pmatrix}. \tag{1.12}$$

The σ-matrix is also known as the covariance matrix. In this thesis we define a matched distribution to be a distribution which has a matched covariance matrix (see Sec. 1.5). A measure for the bunch quality is often given by the its emittance ε_i with $i \in [x, z, l]$, which is given by

$$E_i = \pi \varepsilon_i = \sqrt{\langle i^2 \rangle \langle i'^2 \rangle - \langle ii' \rangle}. \tag{1.13}$$

Since we expect small deviations from the reference orbit s, the preferred units for x, z and l are given in mm, and so are the beams sizes. The deviations of momentum are often given in $mrad$ and the total relative moment deviation in so called *promille*. Thus the units of the emittance are given in π mm $mrad$.

1.1.5 Tracking methods

The two approaches for tracking particles in any system of interest are the so called *particle-in-cell*(PIC) and the $transfer\text{-}map$ method. The advantage of PIC simulations is that all the strengths of the computer experiment can be reached out. These are namely the completeness of numerical calculations, where non-linearity, many degrees of freedom and maybe lack of symmetry can be considered. Because of this, the PIC method was addressed as a high fidelity model. Of course this translates into a higher computational cost, both during the simulation, as well as during the analysis of the data. In contrast the transfer maps are our surrogate model, which allows us to make interesting predictions of the system. All in all, we start by describing the underlying theory of the transfer maps and then briefly present the PIC method used in OPAL.

1.2 Modern map theory

Although the modern map theory is based on the study of Lie Algebras, we avoid that formalism and concentrate on the practical computation of a transfer map, which is rooted on Hamilton mechanics. The linear transfer map method has shown to be inefficient in cases were high order instabilities arise mostly due to imperfections in external electromagnetic fields and/or collective effects. It is also worth mentioning that the linear transfer map methods are still widely used, and they are a central part of the computation of a matched distribution. On this regard the modern map theory is a generalization, which contains also the non-linear transfer maps and can be a powerful tool to study higher order aberrations in ion optics.

1.2.1 On the Hamilton formalism and the transfer map

In this subsection the formula to compute a transfer map is presented. Therefore we start with some universal concepts. In a very general way, we consider canonical pairs (q_i, p_i), $i \in [1, 2, 3]$, where q_i are the spatial coordinates and p_i are their canonical conjugates, the momentum coordinates. We are interested on the evolution of the system over time and more importantly, we would like to know how the system looks at a specific time t given some initial conditions at t_0. In other words, we would like to know if there is a function $f(\vec{q}, \vec{p}, t)$ such that

$$\frac{d}{dt}\begin{pmatrix}\vec{q}\\ \vec{p}\end{pmatrix} = f(\vec{q}, \vec{p}, t), \tag{1.14}$$

and also the vector satisfies the initial condition $(\vec{q}(t_0)\ \vec{p}(t_0))^T = (\vec{q}_0\ \vec{p}_0)^T$. This has been a central question, which has motivated a lot of studies in the field of differential equations and of course physics. The concept of a transfer map $\mathcal{M}$ is in a sense close to the problem at hand. We would like to know if there is a function $\mathcal{M}$, such that it satisfies

$$\begin{pmatrix}\vec{q}(t_1)\\ \vec{p}(t_1)\end{pmatrix} = \mathcal{M}(\vec{q}(t_0), \vec{p}(t_0), t_0, t_1). \tag{1.15}$$

In other words, we would like to know if there is a function $\mathcal{M}$ (also known as propagator) such that given the initial conditions at t_0 it can return the state vector at time t_1. It give us the comodity of iteration, so to speak. We can intuitively generate component-wise the function f from Eq. 1.14 with help from the Hamiltonian H,

$$\frac{\partial H}{\partial p_i} = \dot{q}_i \qquad\qquad \frac{\partial H}{\partial q_i} = -\dot{p}_i. \tag{1.16}$$

We can write this equations in the more compact and practical form

$$\frac{d}{dt}\begin{pmatrix}\vec{q}\\ \vec{p}\end{pmatrix} = \begin{pmatrix}\partial H/\partial \vec{p}\\ -\partial H/\partial \vec{q}\end{pmatrix} = \hat{J}\begin{pmatrix}\partial H/\partial \vec{q}\\ \partial H/\partial \vec{p}\end{pmatrix}, \tag{1.17}$$

where the matrix $\hat{J}$ is given by

$$\hat{J} = \begin{pmatrix}\hat{0} & \hat{I}\\ -\hat{I} & \hat{0}\end{pmatrix},$$

with $\hat{I}$ the identity matrix and $\hat{0}$ represents the zero matrix. Now that we know how the differential equations of our system look, we might recognize that building a transfer map $\mathcal{M}$ would be extremely practical for the purpose of studying the evolution of the system. In fact we see that the Hamiltonian is closely related to it, since it dictates the differential equations of motion.

At this point it becomes unavoidable to introduce the so-called Lie-product and the Lie-transformation. The Lie-product is a binary operation on elements of a linear vector space, in our case, the vector space is the set of all functions of the variables $\vec{q}, \vec{p}, t$. Let then f and g be functions of this set, then we define the Lie product by the Poisson bracket

$$[f, g] := \sum_{i=1}^{3} \frac{\partial f}{\partial q_i}\frac{\partial g}{\partial p_i} - \frac{\partial f}{\partial p_i}\frac{\partial g}{\partial q_i}. \tag{1.18}$$

Although for heuristic reasons the formalities of a Lie algebra won't be presented, it is worth remarking that a vector space together with a Lie product is called a Lie algebra. A Lie product does not have to be the Poisson bracket. In our particular case we are bound to the study of the so called *Poisson Bracket Lie algebra of dynamical variables*.

We also define now the Lie operator

$$: f : := \sum_{i=1}^{3} \frac{\partial f}{\partial q_i}\frac{\partial}{\partial p_i} - \frac{\partial f}{\partial p_i}\frac{\partial}{\partial q_i}, \tag{1.19}$$

such that

$$: f : g = [f, g]. \tag{1.20}$$

Also this Lie operator is bounded to a so called Lie transformation given by

$$\exp(: f :) = \sum_{n=0}^{\infty} \frac{: f :^n}{n!}. \tag{1.21}$$

Now we have the necessary ingredients to make the connection between the map $\mathcal{M}$ and the Hamiltonian H. First we can directly recognize that

$$\dot{q}_i = - : H : q_i, \qquad\qquad \dot{p}_i = - : H : p_i, \tag{1.22}$$

we see that the Poisson bracket $- : H :$ contains the information we need to generate the equations of motion. We shall remark that the following equation is a direct consequence of the theorems 4.1 and 4.2 from Chapter 6 Section 4 of [5]. Lastly the transfer map $\mathcal{M}$ of a Hamiltonian H is given by the Lie transformation, given that the Hamiltonian is not explicitly dependent on time (*autonomous*)

$$\mathcal{M} = \exp((t - t_0) : -H :),$$

or since we can make a direct transformation of the independent variable t

$$\mathcal{M} = \exp(-(s - s_0) : H :) = \exp(-\Delta s : H :). \tag{1.23}$$

It then follows that

$$\begin{pmatrix} \vec{q}(s) \\ \vec{p}(s) \end{pmatrix} = \mathcal{M} \begin{pmatrix} \vec{q}(s_0) \\ \vec{p}(s_0) \end{pmatrix} = \exp(-\Delta s : H :) \begin{pmatrix} \vec{q}(s_0) \\ \vec{p}(s_0) \end{pmatrix}$$

Furthermore any *autonomous* Hamiltonian H produces a so called symplectic map, which translates into following relation

$$J = \mathcal{M}^T J \mathcal{M}. \tag{1.24}$$

1.3 Linear transfer maps

With Eq. 1.23 we can now generate transfer maps for any given *autonomous* Hamiltonian H. The following step is to generate a suitable Hamiltonian H for our system to compute the transfer map. The following subsection, shows a derivation of a simplified Hamiltonian and presents the approximations taken in account. After that we proceed to compute the transfer maps in linear approximation.

1.3.1 Equations of motion and a simplified Hamiltonian

The equations of motion can be directly derived from the well known relativistic Hamiltonian of a charged particle under the influence of electromagnetic fields

$$H = \sqrt{(\vec{p} - q\vec{A})^2 + (mc^2)^2} + Q\phi, \tag{1.25}$$

where m represents the mass of the particle, Q the charge of the particle, c the speed of light, ϕ and $\vec{A}$ are the electric and magnetic potentials respectively and $\vec{p}$ is the momentum. This Hamiltonian yields the also well known Lorentz force

$$\vec{F} = \gamma m\ddot{\vec{q}} = Q(\vec{E} + \dot{\vec{q}} \times \vec{B}), \tag{1.26}$$

where $\vec{E}$ and $\vec{B}$ are the electric and magnetic fields. Applying canonical transformations, we can write Eq. 1.21 in our coordinate system

$$H = -(1+hx)\sqrt{\left(\frac{1}{\beta} + \delta - \frac{q\phi}{p_0 c}\right)^2 - (p_x - a_x)^2 - (p_z - a_z)^2 - \frac{1}{(\beta\gamma)^2}} - (1+hx)a_l + \frac{\delta}{\beta}, \tag{1.27}$$

where $h = 1/\rho$ is the inverse bending radius or curvature and p_0 is the reference momentum at s. The transformed magnetic potential $\vec{a}$ (does not have anything to do with the cyclotron length from Eq. 1.6) is given by

$$\vec{a} = \frac{Q}{p_0}\vec{A}.$$

Details on the derivation of this Hamiltonian can be found in [6]. Since we want to apply our Lie operator from Eq. 1.19 to compute the transfer map, this Hamiltonian becomes difficult to deal with. For this reason we consider the following approach.

Reconsider now the system at hand, where we would like to track a particle in an accelerator with an external magnetic field $\vec{B}(s)$ along the acompanying coordinate system, thus the system is bound to a zentripetal force. In [4] a very practical derivation of the equations of motion in linear approximation is presented. The derivation, takes following considerations, note that the vectors dependent on s refer to the accompanying coordinate system and the vectors dependent on t are the ones on laboratory system.
First the external magnetic field $\vec{B}$ is given by

$$\vec{B} = B_0 \begin{pmatrix} nhz \\ 1 - nhx \\ 0 \end{pmatrix}, \tag{1.28}$$

where $B_0 = B(s)$ is the nominal magnetic field and n is the negative field index (the difference arises from a convention). This is nothing else than the linear expansion of the magnetic field around $(x(s) = 0, z(s) = 0)$. On the other hand we know that the centripetal acceleration is

given by $a_r = -\omega^2(\rho + x(s))$. We also take into consideration that the velocity $v_l \gg v_x, v_z$ such that $|\vec{v}| \approx v_l$. It then follows that

$$p = |\vec{p}| = \gamma m |\vec{v}| \approx \gamma m v_l = \gamma m \omega(\rho + x(s)). \tag{1.29}$$

Hence the equations of motion are

$$\ddot{\vec{x}} - \omega^2(\rho + x(s))\vec{e_x} = \frac{Q}{m}(\vec{v} \times \vec{B}), \tag{1.30}$$

which componentwise reads

$$\ddot{x} = -Q v_l B_z + \omega^2(\rho + x(s)), \tag{1.31}$$

$$\ddot{z} = Q v_l B_x. \tag{1.32}$$

Taking into consideration the approximations above, together with $ds/dt = \rho\omega$ and dividing the equations by $(\rho\omega)^2$ we obtain:

$$x'' = -\frac{QB_0}{p}(1 - nhx)(1 + xh)^2 + h(1 + xh), \tag{1.33}$$

$$z'' = -\frac{QB_0}{p} nhz(1 + hx)^2. \tag{1.34}$$

The last approximation made, takes in account the relative moment difference δ

$$\frac{1}{p} = \frac{1 - \delta}{p_0} = \frac{1 - \delta}{QB_0\rho}. \tag{1.35}$$

We can immediately recognize that Eq. 1.33 and 1.34 contain higher order terms in x, as well as mixed terms with the form $x\delta$, $z\delta$ and xz. Taking in account just the terms linear in x, z and δ yields

$$x'' + (1 - n)h^2 x = \delta h, \tag{1.36}$$

$$z'' + nh^2 z = 0. \tag{1.37}$$

These equations show that the motion of a particle around the reference orbit is nothing else than a coupled harmonic in the radial direction and a simple harmonic oszillation on the vertical plane in linear approximation. For this end the following focusing strengths k_x, k_z are introduced

$$k_x = (1 - n)h^2, \qquad k_z = nh^2. \tag{1.38}$$

In order to build a proper Hamiltonian we use the equation of motion from [4] Section 4.4.3

$$l' = -hx + \frac{\delta}{\gamma^2}. \tag{1.39}$$

With Eqs. 1.36, 1.37 and 1.39 we can describe the motion in a particle accelerator, if we know the quantities h, n and γ.
On a last step we consider that having a single particle could be experimentally very challenging and also not very appealing for any application. Instead of simulating the cyclotron on a single particle level which is very time consuming, we simulate the motion of bunches. To model the motion of a particle in a bunch, we could go back to Eq. 1.22 and derive again the equations of motion but now taking into consideration both the external magnetic field $\vec{B}$ and the fields $\vec{E}_{sc}$

and $\vec{B}_{sc}$ originated from the bunch space charge distribution. To avoid this, it was implicitly suggested in [1] to introduce in the equations of motion some defocusing strengths K_x, K_z and K_l. With this, the equations of motion of a particle in a bunch yield

$$x'' = (K_x - k_x)x + h\delta, \tag{1.40}$$
$$z'' = (K_z - k_z)z, \tag{1.41}$$
$$l' = -hx + \frac{\delta}{\gamma^2}, \tag{1.42}$$
$$\delta' = \gamma^2 K_l l, \tag{1.43}$$

which finally let us compute the following simplified Hamiltonian

$$H = \frac{x'^2}{2} + \frac{k_x - K_x}{2}x^2 + \frac{z'^2}{2} + \frac{k_z - K_z}{2}z^2 - \frac{\gamma^2 K_l}{2}l^2 + \frac{\delta^2}{2\gamma^2} - hx\delta. \tag{1.44}$$

The defocussing strengths are calculated the same way as in [4] presented in Chapter 11.4. Hence given by

$$K_x = \frac{K_3(1-f)}{(\sigma_x + \sigma_l)\sigma_x\sigma_l}, \tag{1.45}$$
$$K_z = \frac{K_3(1-f)}{(\sigma_x + \sigma_l)\sigma_z\sigma_l}, \tag{1.46}$$
$$K_l = \frac{K_3 f}{\sigma_x\sigma_z\sigma_l}, \tag{1.47}$$

here $\sigma_{x,z,l}$ represent the bunch dimensions, K_3 is the 3 dimensional space charge parameter

$$K_3 = \frac{3QI\lambda}{20\sqrt{5}\pi\epsilon_0 mc^3\beta^2\gamma^2},$$

where I is the current, c is the speed of light, $\lambda = \frac{2\pi c}{\omega_0 N_h}$ is a characteristic wavelength of the system, N_h the harmonic number and ϵ_0 is the vacuum permittivity.
f is the so called form factor and can be approximated by

$$f \approx \frac{\sqrt{\sigma_x\sigma_l}}{3\gamma\sigma_z}.$$

1.3.2 Transfer matrices

With the help from Eq. 1.23 and the simplified Hamiltonian (Eq. 1.44) we can directly build the transfer map $\mathcal{M}$. These quantities K_x, K_z and K_l depend on the bunch size, but the bunch size depends also on these quantities. To solve this problem, following approximation was taken in [2], taking advantage of the Baker-Campbell-Hausdorff formula

$$\begin{aligned}\mathcal{M} = \exp\left(-\Delta s : H :\right) &= \exp\left(-\Delta s : H_{sc} + H_{cyc} :\right) \\ &= \exp\left(-\Delta s : H_{sc} : -\Delta s : H_{cyc} :\right) \\ &= \exp\left(-\Delta s : H_{sc} :\right)\exp\left(-\Delta s : H_{cyc} :\right) + \mathcal{O}(\Delta s^2), \end{aligned} \tag{1.48}$$

where we applied a separation of the Hamiltonian such that

$$H = H_{sc} + H_{cyc} \tag{1.49}$$

with

$$\begin{aligned} H_{cyc} &= \frac{x'^2}{2} + \frac{k_x}{2}x^2 + \frac{z'^2}{2} + \frac{k_z}{2}z^2 + \frac{\delta^2}{2\gamma^2} - hx\delta, \\ H_{sc} &= -\left(\frac{K_x}{2}x^2 + \frac{K_z}{2}z^2 + \frac{\gamma^2 K_l}{2}l^2\right). \end{aligned}$$

This method allows us to apply a transfer map $\mathcal{M}_{cyc}$ to the particles of the bunch and then with the resulting bunch sizes we can build the transfer map $\mathcal{M}_{sc}$. As discussed in [7], a common practice by the computation of the transfer maps is to truncate the series of expansion described by Eq. 1.21. Reasons for truncation are often because no closed form can be found, for numerical, performance and/or precision reasons. Naturally this compromise breaks in general the symplectic condition described by Eq. 1.24. At this point we analogously truncate the expansion series to first order, such that

$$\mathcal{M} = \sum_{n=0}^{\infty} \frac{(-\Delta s : H :)^n}{n!} = \hat{I} - \Delta s : H : +\mathcal{O}(\Delta s^2), \tag{1.50}$$

thus, we use transfer maps in linear approximation.

Applying Eq. 1.50 together with 1.19 we get for $: H_{cyc} : \vec{x}$

$$\begin{aligned}
: H_{cyc} : x &= \frac{\partial H_{cyc}}{\partial x}\frac{\partial x}{\partial x'} - \frac{\partial H_{cyc}}{\partial x'}\frac{\partial x}{\partial x} + \frac{\partial H_{cyc}}{\partial z}\frac{\partial x}{\partial z'} - \frac{\partial H_{cyc}}{\partial z'}\frac{\partial x}{\partial z} + \frac{\partial H_{cyc}}{\partial l}\frac{\partial x}{\partial \delta} - \frac{\partial H_{cyc}}{\partial \delta}\frac{\partial x}{\partial l} = -x', \\
: H_{cyc} : x' &= \frac{\partial H_{cyc}}{\partial x}\frac{\partial x'}{\partial x'} - \frac{\partial H_{cyc}}{\partial x'}\frac{\partial x'}{\partial x} + \frac{\partial H_{cyc}}{\partial z}\frac{\partial x'}{\partial z'} - \frac{\partial H_{cyc}}{\partial z'}\frac{\partial x'}{\partial z} + \frac{\partial H_{cyc}}{\partial l}\frac{\partial x'}{\partial \delta} - \frac{\partial H_{cyc}}{\partial \delta}\frac{\partial x'}{\partial l} = k_x - h\delta, \\
: H_{cyc} : z &= \frac{\partial H_{cyc}}{\partial x}\frac{\partial z}{\partial x'} - \frac{\partial H_{cyc}}{\partial x'}\frac{\partial z}{\partial x} + \frac{\partial H_{cyc}}{\partial z}\frac{\partial z}{\partial z'} - \frac{\partial H_{cyc}}{\partial z'}\frac{\partial z}{\partial z} + \frac{\partial H_{cyc}}{\partial l}\frac{\partial z}{\partial \delta} - \frac{\partial H_{cyc}}{\partial \delta}\frac{\partial z}{\partial l} = -z', \\
: H_{cyc} : z' &= \frac{\partial H_{cyc}}{\partial x}\frac{\partial z'}{\partial x'} - \frac{\partial H_{cyc}}{\partial x'}\frac{\partial z'}{\partial x} + \frac{\partial H_{cyc}}{\partial z}\frac{\partial z'}{\partial z'} - \frac{\partial H_{cyc}}{\partial z'}\frac{\partial z'}{\partial z} + \frac{\partial H_{cyc}}{\partial l}\frac{\partial z'}{\partial \delta} - \frac{\partial H_{cyc}}{\partial \delta}\frac{\partial z'}{\partial l} = k_z, \\
: H_{cyc} : l &= \frac{\partial H_{cyc}}{\partial x}\frac{\partial l}{\partial x'} - \frac{\partial H_{cyc}}{\partial x'}\frac{\partial l}{\partial x} + \frac{\partial H_{cyc}}{\partial z}\frac{\partial l}{\partial z'} - \frac{\partial H_{cyc}}{\partial z'}\frac{\partial l}{\partial z} + \frac{\partial H_{cyc}}{\partial l}\frac{\partial l}{\partial \delta} - \frac{\partial H_{cyc}}{\partial \delta}\frac{\partial l}{\partial l} = -\frac{\delta}{\gamma^2} + hx, \\
: H_{cyc} : \delta &= \frac{\partial H_{cyc}}{\partial x}\frac{\partial \delta}{\partial x'} - \frac{\partial H_{cyc}}{\partial x'}\frac{\partial \delta}{\partial x} + \frac{\partial H_{cyc}}{\partial z}\frac{\partial \delta}{\partial z'} - \frac{\partial H_{cyc}}{\partial z'}\frac{\partial \delta}{\partial z} + \frac{\partial H_{cyc}}{\partial l}\frac{\partial \delta}{\partial \delta} - \frac{\partial H_{cyc}}{\partial \delta}\frac{\partial \delta}{\partial l} = 0,
\end{aligned}$$

which reads in matrix form

$$: H_{cyc} : \vec{x} = \begin{pmatrix} 0 & -1 & 0 & 0 & 0 & 0 \\ k_x & 0 & 0 & 0 & 0 & -h \\ 0 & 0 & 0 & -1 & 0 & 0 \\ 0 & 0 & k_z & 0 & 0 & 0 \\ h & 0 & 0 & 0 & 0 & -\frac{1}{\gamma^2} \\ 0 & 0 & 0 & 0 & 0 & 0 \end{pmatrix} \begin{pmatrix} x \\ x' \\ z \\ z' \\ l \\ \delta \end{pmatrix}.$$

Hence is the transfer map in linear approximation

$$\mathcal{M}_{cyc} = \hat{I} + F_{cyc}\Delta s, \tag{1.51}$$

with

$$F_{cyc} = \begin{pmatrix} 0 & 1 & 0 & 0 & 0 & 0 \\ -k_x & 0 & 0 & 0 & 0 & h \\ 0 & 0 & 0 & 1 & 0 & 0 \\ 0 & 0 & -k_z & 0 & 0 & 0 \\ -h & 0 & 0 & 0 & 0 & \frac{1}{\gamma^2} \\ 0 & 0 & 0 & 0 & 0 & 0 \end{pmatrix}.$$

In a similar way we can compute the transfer map for H_{sc}, which leads us to

$$\mathcal{M}_{sc} = \hat{I} + F_{sc}\Delta s, \tag{1.52}$$

with

$$F_{sc} = \begin{pmatrix} 0 & 0 & 0 & 0 & 0 & 0 \\ K_x & 0 & 0 & 0 & 0 & 0 \\ 0 & 0 & 0 & 0 & 0 & 0 \\ 0 & 0 & K_z & 0 & 0 & 0 \\ 0 & 0 & 0 & 0 & 0 & 0 \\ 0 & 0 & 0 & 0 & K_l\gamma^2 & 0 \end{pmatrix}.$$

The transport of a particle in a cyclotron is then given by the simple matrix multiplication

$$\vec{x}_f = \mathcal{M}_{sc}\mathcal{M}_{cyc}\vec{x}_0. \tag{1.53}$$

If we know the initial vectors $\vec{x}_0$ from every particle in the bunch, we can compute their transport and with this information, we can compute the beam dimensions. Consider now that the nominal current at the PSI cyclotron is $I = 2.19$mA. That means, a bunch would contain $N \approx 10^8$ protons. This makes the transport of single particle inconvinient. For this reason we compute the initial σ-matrix and transport it analogously with the help of the transfer map in the following manner

$$\sigma_f = \mathcal{M}\sigma_0\mathcal{M}^T. \tag{1.54}$$

From now on we refer to the transfer maps in linear approximation $\mathcal{M}$ as transfer maps or simply transfer matrices.

1.4 OPAL tracking

Now that we have described, how to track particles with help of transfer maps, the PIC-method should be briefly discussed. The concepts described in the following sections are based on [8] and [9].

1.4.1 Particle-particle method

As before, a very intuitive and simple way to model and predict the behaviour of a physical system composed of N particles is to compute the state of the physical system, which is given by the particle positions and momenta (q_i, p_i) for $i \in [0, 1, ..., N]$ for a given time t. In the particle-particle (PP) method the concept of *action at a distance* is prioretized, meaning that the force acting on the ith-particle at a certain time t is given by

$$\vec{F}_i = \dot{\vec{p}}_i = \sum_{i \neq j}^{N} \vec{F}_{i,j} + \vec{F}_{ext,i} = \sum_{i \neq j}^{N} \vec{F}_{i,j}(\vec{q}_i, \vec{q}_j) + \vec{F}_{ext,i}(\vec{q}_i, \vec{p}_i). \tag{1.55}$$

With this in mind we might already intuit, that this approach is rather inefficient for systems with large N. Therefore the PP method is limited by its computational efficiency. For large systems where the number of particles is above $N > 10^6$, even running such algorithms on modern state of the art computers is inefficient and intesively time and memory consuming.

1.4.2 Particle-mesh method

The particle mesh (PM) method exploits the concept of $force\ at\ a\ point$. From a physical point of view it is equivalent to the PP approach, with the difference that the force F_i is now given as a field equation, for example Eq. 1.26,

$$\vec{F}_i = Q[\vec{E}(\vec{q}_i) + \dot{\vec{q}}_i \times \vec{B}(\vec{q}_i)].$$

In other words the interaction is now quantified and discretized with field quantities dependent on the position of the particle. The size of the mesh is important for the resolution of the phenomena, which might be studied. This approach is generally less accurate but more efficient and known as particle in cell (PIC) method.

1.4.3 Bunch tracking in OPAL

In order to track a bunch of particles in the system of interest, it is practical to consider again the density distribution $f(q, \dot{q}, t)$ of the particles in extended phase space. Still the number of particles is very high and for this, the user can input the number of macroparticles that are sampled by f. Then in OPAL the evolution of this density distribution over time is computed with the help of the Vlassov equation

$$\frac{df}{dt} = \frac{\partial f}{\partial t} + \dot{\vec{q}} \nabla_q f + Q(\vec{E} + \dot{\vec{q}} \times \vec{B}) \nabla_{\dot{q}} f = 0. \tag{1.56}$$

The simulation can be started with different types of distributions. OPAL in its standard mode can generate particles from a file containing $(q_i, \dot{q}_i)$ or generate a collection of particles, given the wished values for the standard deviations $(\sigma_{q_i}, \sigma_{\dot{q}_i})$ and correlations. Also the type of distribution can be chosen, ranging from a standard 6D-Gaussian, to the Kapchinscky-Vladimirsky (KV) and waterbag distributions.

The numerical scheme has the following approach. The electromagnetic fields can be separated into two parts, one part including the external fields, which have to be given by the user, and the other part given by the fields due to the charge distribution of the bunch

$$\vec{E} = \vec{E}_{ext} + \vec{E}_{sc}, \qquad \vec{B} = \vec{B}_{ext} + \vec{B}_{sc}. \tag{1.57}$$

In order to compute the later part of the fields, OPAL applies a proper Lorentz transformation $\mathcal{L}$ to the bunch coordinates, such that a quasi-static bunch, with only $\vec{E}_{sc}$ part, can be computed. Then the Poisson eq. is solved

$$-\Delta\phi = \frac{\mathcal{L}(\rho(x,z,l))}{\epsilon_0}, \tag{1.58}$$

where $\rho(x,y,l)$ is the density space charge distribution given by the user and ϕ is the electric potential. Then the electric field is computed $\vec{E'} = -\vec{\nabla}\phi$ and backtransformed to laboratory system. With this simulation scheme, the evolution of the bunch in the cyclotron has been studied in detail. The challenges in the implementation arise of course on the discretization of Eq. 1.56, as well as in the solving process of Eq. 1.58. For more details refer to [9] and [10].

1.5 Matched distributions

As presented on Section 1.3.2 the transport of the σ-matrix can be computed with Eq. 1.54. A very interesting subject of study are the so called matched distributions. Recalling our definition of matched distribution from Section 1.1.4, we defined a matched distribution as a collection of particles, whose probability density function has a matched covariance matrix. To define what a matched covariance matrix is, consider the following. Suppose we know for a given configuration (energy of the bunch, number of particles, field map of the system , etc.) the equilibrium closed orbit in the cyclotron. Then, for each path length of the equilibrium orbit Δs_i with $i \in [1,2,3,...,N]$ the one turn transfer map $\mathcal{M}_\mathcal{T}$ is given by

$$\mathcal{M}_\mathcal{T} = \prod_{i=1}^{N} \mathcal{M}_i = \mathcal{M}(\Delta s_N) \cdot \mathcal{M}(\Delta s_{N-1}) \cdot ... \cdot \mathcal{M}(\Delta s_1). \tag{1.59}$$

Hence a matched covariance matrix should fulfill the following relation

$$\sigma_M = \mathcal{M}_\mathcal{T} \sigma_M \mathcal{M}_\mathcal{T}^T. \tag{1.60}$$

In other words, the convariance matrix remains invariant if applying the one turn transfer matrix $\mathcal{M}_\mathcal{T}$. The computation and study of matched distributions is imperative in particle accelerators. These distributions should be stable in the system and the calculation of matched distributions has also been addressed as the storage ring problem. The existence of these translates in to a measure about the stability of the system for a given configuration, for instance we can know the space charge limit or the stable higher amount of particles we can have in a coasting bunch. In a N symmetric system, such as an N sector cyclotron, computing a matched distribution for one sector transfer matrix should be enough to find a stable coasting beam.

For a system where space charge effects can be neglected, there is no need of Eq. 1.48, thus making the computation straighforward. In the following section we present a method to find and compute matched distributions. Then we assess if the computed matched distributions are indeed matched if we take in account higher order instabilities, which are modelled with help from the PIC method in OPAL.

1.5.1 Computation of a matched distribution

In [11] it has been shown that for a diagonalizable and symplectic one turn transfer matrix $\mathcal{M}_\mathcal{T}$ i.e. the transfer matrix fulfills Eq. 1.24 and can be written in the form

$$\mathcal{M}_\mathcal{T} = E\Lambda E^{-1}, \tag{1.61}$$

where E is the matrix containing the eigenvectors and Λ is the diagonal matrix containing the eigenvalues of $\mathcal{M}_\mathcal{T}$. Then the matched covariance matrix can be computed with following relation

$$\sigma_M = -EDE^{-1}S, \tag{1.62}$$

where $D = \text{diag}(i\varepsilon_x, -i\varepsilon_x, i\varepsilon_z, -i\varepsilon_z, i\varepsilon_l, -i\varepsilon_l)$ and S is the skew-matrix

$$S = \begin{pmatrix} \tilde{I} & \hat{0} & \hat{0} \\ \hat{0} & \tilde{I} & \hat{0} \\ \hat{0} & \hat{0} & \tilde{I} \end{pmatrix},$$

with $\tilde{I} = \begin{pmatrix} 0 & 1 \\ -1 & 0 \end{pmatrix}$.

Based on Eqs. 1.61 and 1.62 an algorithm in OPAL was implemented to compute such matched covariance matrices. First the algorithm computes the equilibrium closed orbit for the desired energy of the bunch, such that the quantities h, n and γ could be known for every point in s. Thus, the one turn transfer matrix reads

$$\mathcal{M}_\mathcal{T} = \prod_{i=1}^{N} \mathcal{M}_i = \mathcal{M}_{sc}(\Delta s_N)\cdot\mathcal{M}_{cyc}(\Delta s_N)\cdot\mathcal{M}_{sc}(\Delta s_{N-1})\cdot\mathcal{M}_{cyc}(\Delta s_{N-1})\cdot\ldots\cdot\mathcal{M}_{sc}(\Delta s_1)\cdot\mathcal{M}_{cyc}(\Delta s_1) \tag{1.63}$$

with stepsize $\Delta s_i = \sqrt{(\frac{dr}{d\theta})^2 + r^2}\Delta\theta_i$, with equidistant angular steps $\Delta\theta_i = \frac{2\pi i}{N}$. A complication arises when trying to compute $\mathcal{M}_{sc}(\Delta s_i)$ since we don't know the matched distribution, we are not able to compute the one turn transfer matrix and vice versa.

For this reason an iterative process was suggested in [1]. Namely, to initialize a spherical distribution with the σ-matrix

$$\sigma_{init} = \frac{1}{B-A}\begin{pmatrix} \frac{B\varepsilon_x}{\Omega} + \frac{A\varepsilon_l}{\omega} & 0 & 0 & 0 & 0 & \frac{\varepsilon_x}{\Omega} + \frac{\varepsilon_l}{\omega} \\ 0 & B\varepsilon_x\Omega + A\varepsilon_l\omega & 0 & 0 & \frac{\varepsilon_x\Omega+\varepsilon_l\omega}{K\gamma^2} & 0 \\ 0 & 0 & \frac{\varepsilon_z}{\sqrt{h^2\nu_z^2-K}} & 0 & 0 & 0 \\ 0 & 0 & 0 & \frac{\varepsilon_z}{\sqrt{h^2\nu_z^2-K}} & 0 & 0 \\ 0 & \frac{\varepsilon_x\Omega+\varepsilon_l\omega}{K\gamma^2} & 0 & 0 & \frac{A\varepsilon_x\Omega+B\varepsilon_l\omega}{K\gamma^2} & 0 \\ \frac{\varepsilon_x}{\Omega} + \frac{\varepsilon_l}{\omega} & 0 & 0 & 0 & 0 & \frac{\varepsilon_x}{B\Omega} + \frac{\varepsilon_l}{A\omega} \end{pmatrix} \tag{1.64}$$

with

$$\begin{aligned} A &= \frac{h}{\Omega^2 + K}, \\ B &= \frac{h}{\omega^2 + K}, \\ \Omega^2 &= a + \sqrt{a^2 - K^2}, \\ \omega^2 &= a - \sqrt{a^2 - K^2}, \\ a &= \frac{h^2\gamma^2}{2} - K \end{aligned}$$

where

$$K = K_x = K_z = K_l = \frac{K_3 \gamma}{3\sigma^3}$$

with the approximation

$$\sigma = \begin{cases} \sigma_0(1 + \frac{\alpha}{4} - \frac{\alpha^2}{32}) & \text{for } 0 \leq \alpha \leq 2.5 \\ \sigma_0 \sqrt[3]{1+\alpha} & \text{for } 2.5 \leq \alpha \end{cases} \tag{1.65}$$

with

$$\begin{aligned} \alpha &= \frac{q\mu_0 I}{5\sqrt{10}mc\gamma N_h}\sqrt{\frac{a}{\bar{\varepsilon}}}, \\ \sigma_0 &= \frac{\sqrt{2a\bar{\varepsilon}}}{\gamma}, \\ \bar{\varepsilon} &= \sqrt[3]{\varepsilon_x \varepsilon_z \varepsilon_l} \end{aligned}$$

where a in σ_0 is the cyclotron length from Eq. 1.6. With this first guess for the σ-matrix, we are able to construct the one turn transfer map $\mathcal{M}_\mathcal{T}$. With $\mathcal{M}_\mathcal{T}$ and Eq. 1.62, we update our initial guess distribution σ_{init}, until the matrix doesn't change anymore. The algorithm then looks something like this

1. Compute a closed orbit for the desired energy E in order to calculate the quantities h, n, etc.
2. Initialize $\sigma_{init,0}$ with help of Eq. 1.64.
3. Compute the transfer maps $\mathcal{M}_{sc}$ for each step Δs_i with $i \in [1, 2, ..., N]$
4. Compute the one turn transfer map $\mathcal{M}_\mathcal{T}$
5. Compute $\sigma_{init,new}$ with help of Eq. 1.62.
6. If $\sigma_{init,new}$ is up to a numerical threshold the same as $\sigma_{init,0}$ then stop, if not, go back to Step 3 with an updated $\sigma_{init,0} = w\sigma_{init,new} + (1-w)\sigma_{init,0}$.

In the next chapter, this scheme is applied to the cyclotrons at PSI, and then the limitations of the model are assessed by comparing the results with the PIC tracking algorithm described before. The numerical threshold takes into consideration the L_2-Norm of the difference between $\sigma_{init,new}$ and $\sigma_{init,0}$. The weight w is a user defined parameter and was set to $w = 0.65$. Another important aspect of the algorithm is that the emittances $\varepsilon_{x,z,l}$ in Eq. 1.62 that build the matrix D are also user defined and is an important degree of freedom, since varying this parameter leads to different results. In this thesis, we restrain to the case $\varepsilon_x = \varepsilon_z = \varepsilon_l$.

Chapter 2

Simulation and Results

First we describe the two high intensity cyclotrons at PSI, secondly we compute and evaluate the characteristics of the matched distributions of both machines. At last we compare the results with the OPAL tracking. Most of the descriptions on this chapter are qualitative. A more quantitative assessment of the data is presented in chapter 3.

It is worth mentioning that during this thesis the OPAL framework had the possibility to compute the matched distributions with idealized field maps, such that the cyclotrons were perfectly N symmetric. In this thesis we used the real field maps, where an ideal numerical symmetry in the magnetic field is not present and for this reason the computation of the matched distributions were done with the one turn transfer matrix. OPAL did not have by the beginning of this thesis the feature to later generate and track the distributions. For the algorithm to work with real field maps (generated from measurements) some changes had to be implemented and in this process also some bugs were discovered and fixed.

2.1 High intensity cyclotrons at PSI

The high intensity cyclotrons at PSI are part of the High Intensity Proton Facility or HIPA (for its german acronym). Schematics of the facility are shown on the following Figure.

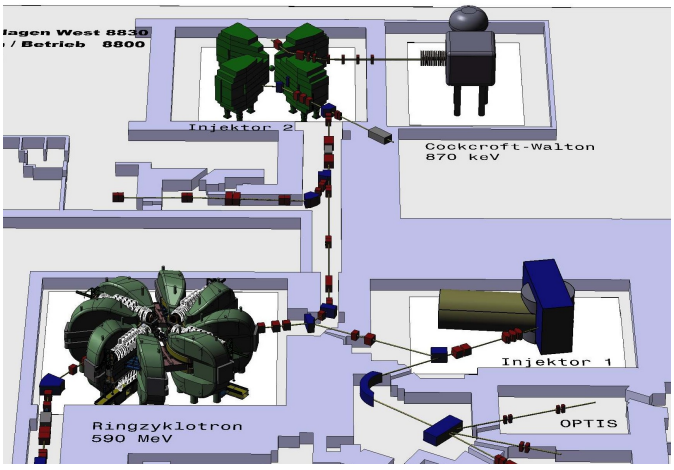

Figure 2.1: The high intensity proton facility at PSI. Source: [21]

The acceleration process of the protons starts at the Cockcroft-Walton electrostatic accelerator (Fig. 2.1 up right), which accelerates the protons obtained from the ion source from 60 keV to 870 keV. Then the protons are transported to second phase of the acceleration, for which the Injector II is responsible. There the protons gain energy from 870 keV to 72 MeV. At last, the protons are taken to the Ring cyclotron, where they reach their end energy of 590 MeV. The proton beam is then ready for use. It can be then conducted to the experimentation hall or be used for the production of secondary particles such as neutrons or muons (which is mostly the case).

2.1.1 Injector II

The Injector II has an injection radius of 0.4m and an extraction radius of 3.5m. The field strength in the midplane (z = 0) is $B_0 = 0.33T$. The magnetic field does not scale, since $\gamma \approx 1$ for protons for this energy range. The bunches move in the cyclotron in counter clockwise direction. The injection energy of the Injector II is at 870keV. The bunches possess an emittance of $\varepsilon \approx 2\pi$ mm mrad. The pre-bunched beam is delivered with a current of 11mA. For this reason, in the first 5 turns of the acceleration the beam is strongly collimated until an operational current of 2.2mA is reached. After the collimation process the beam has an energy of $\sim$ 4MeV. The following Figure the schematics of the Injector are shown, we recognize that the Injector II has 4 sector magnets tagged with "SM1-4", together with 4 high frequency resonators (tagged with "RES1-4" and the color green), which are responsible of the acceleration proccess.

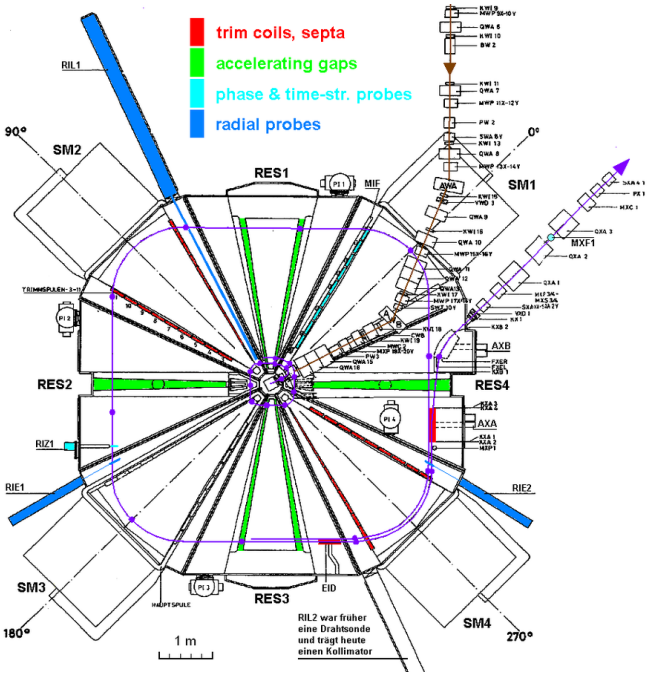

Figure 2.2: Injector II. High intensity cyclotron at PSI. Source:[22]

The injection angle is 30° and it takes 81 turns for the bunch to reach the extraction radius. The cyclotron has an operational frequency $\omega_0 = 50.63$MHz and is driven to the harmonic number $N_h = 10$.

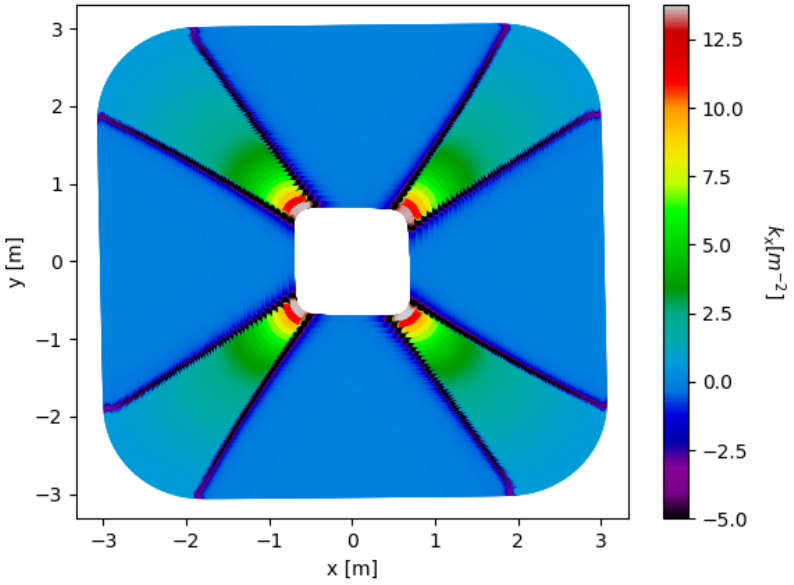

(a)

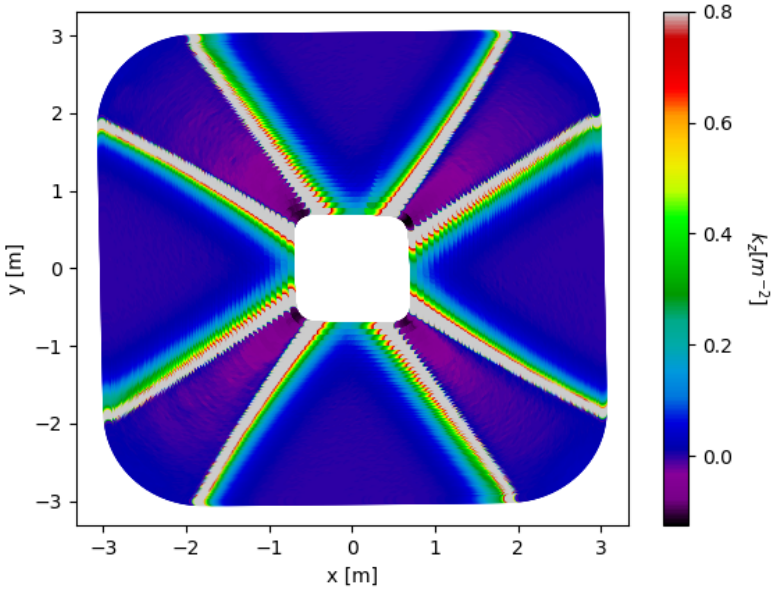

(b)

Figure 2.3: Radial k_x (left) and vertical k_z (right) focussing strengths in Injector II.

We observe that at the edges of the sector magnets the radial direction Fig. 2.3 (a) are defocussed, meanwhile the motion is focussed ($k_x > 0$) as long as the bunch travels through the sector magnets. The vertical direction appears to be at the edges rather strongly focussed Fig. 2.3 (b), but through the sector magnets there is a sligh defocussing effect.

2.1.2 Ring

As presented before the Ring cyclotron has 8 sector magnets and 4 accelerating cavities. It's injection energy is 72MeV and the injection radius is approx. 2m. The injection angle is 110° and it takes 186 turns for the protons to reach the extraction radius of 4.5m. The strength of the magnetic field in the sector magnets yields from 1.8 - 2.17 T. Lastly, the Ring has also the same nominal frequency as the Injector II, but it is driven at a harmonic number $N_h = 6$.

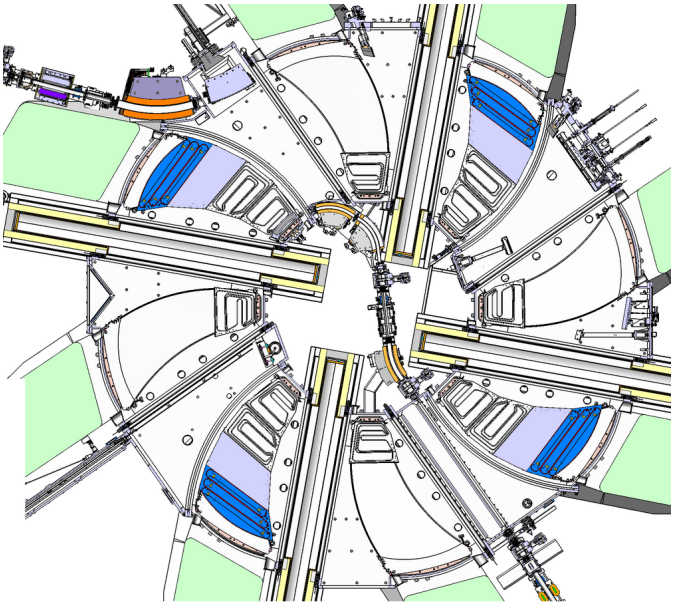

Figure 2.4: The Ring. High intensity cyclotron at PSI. Source: [23]

From Fig. 2.5 we can see that in the Ring the low energetic bunches are highly focussed both in radial and vertical directions. At larger radius the bunches see in radial direction when it passes the sector magnet at the edges a defocussing field and inside the magnet a focussing field. For the vertical direction we recognize more or less the opposite behaviour, it is first focussed by entering the sector magnet, through the sector magnet there is no significant effect but at the other edge it is again defocussed.

2.2 Matched distributions

2.2.1 Injector II

Matched distributions were computed for the Injector II for an energy range from 4MeV to 72MeV. The full low energy range wasn't taken into account, since there the beam is highly collimated. The numerical configuration settings were

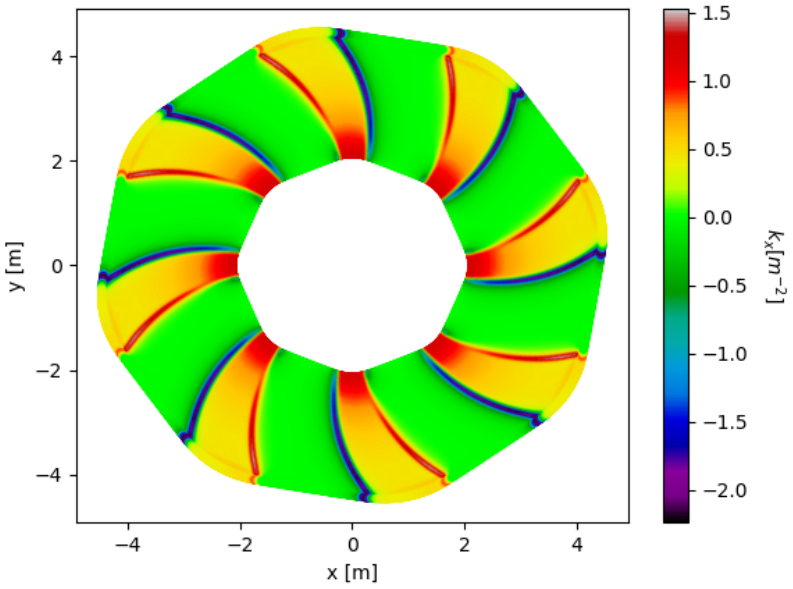

(a)

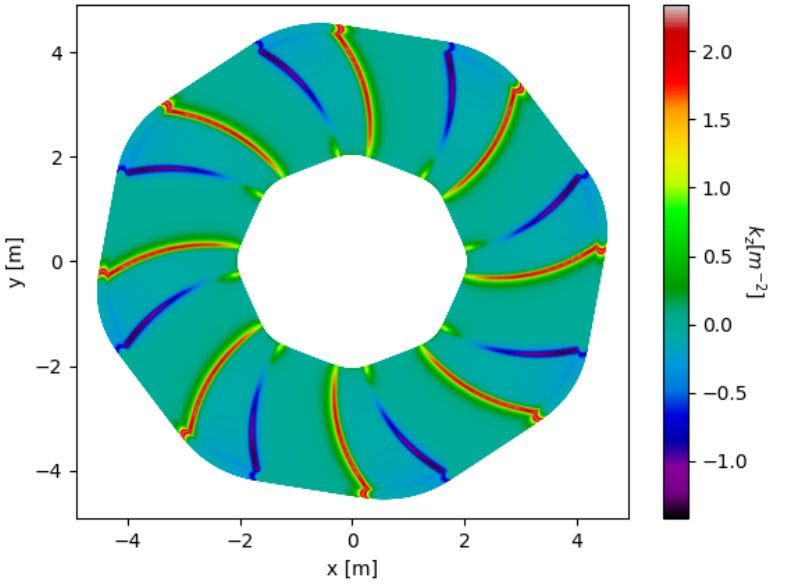

(b)

Figure 2.5: Radial k_x (left) and vertical k_z (right) focussing strengths in the Ring.

Injector II	
energy range [MeV]	4 - 72
energy stepsize [MeV]	1
injection angle ϕ_{init}[°]	30
angular stepsize $\Delta\phi$ [°]	0.25
convergece threshold	10^{-9}
max. # iterations	200
integration scheme	Runge-Kutta 4
emittance ε [π mm mrad]	2
current I [mA]	2.19
# macroparticles N	10000
dump frequency	10

Table 2.1: Numerical setup for Injector II.

Because the uncertainty quantification (UQ) of a simulation is both difficult to determine and an expensive and time consuming process, for this simulation we discuss qualitatively the possible impacts of the numerical parameters from Table 2.1. First the angular stepsize determines the precision of the numerical integration scheme. That means, the smaller $\Delta\phi$, the better precision, at cost of computational power and time. For increasing energy the radius increases as well, this translates in a bigger and bigger stepsize Δs (see Eq. 1.63), meaning that for high energies our precision is poorer than for low energies. Aside from that, another important consideration is that the integration scheme has a precision up to 4th order but it does not conserve energy. This effect is of course small enough, but it can play an important role for large integration ranges. A possible way to avoid this problem is to take e.g. the Leap Frog 2nd order scheme, which conserves energy but has a bigger integration error ($\mathcal{O}(\Delta s^2)$).

The number of macroparticles plays an important role at the time of the generation of the distribution as well as during the PIC simulation. The more macroparticles, the more precise the tracking is but again time, computation and memory considerations led to a moderate N, which is 4 orders of magnitude smaller than the real number of particles. At last the dump frequency determines how often the data is written on a file (positions and momenta of every particle in the bunch). It was chosen to be every 10 integration steps (every 2.5°), because writting every step is both memory and time consuming.

Following beam sizes were found as fuction of the energy.

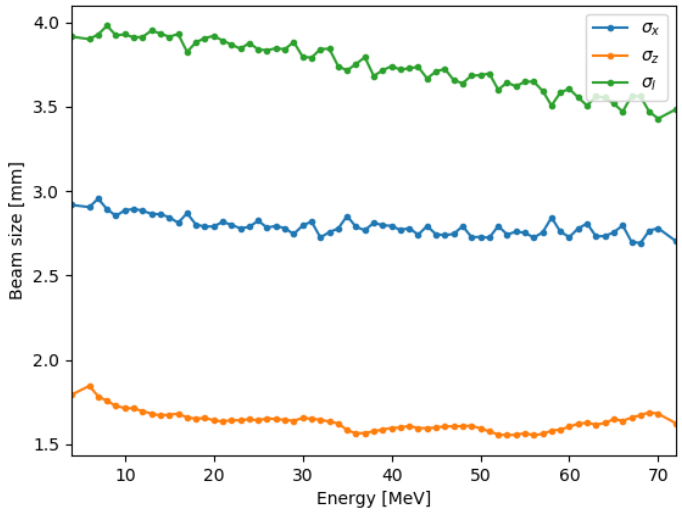

Figure 2.6: 1-σ beam size of the matched distributions at Injector II.

We observed convergence for the complete energy range and Fig. 2.6 shows the beam sizes of the converged covariance matrices. Fig. 2.7 shows a convergence curve, where we can appreciate the numerical threshold diminishing for every iteration. In Fig. 2.8 we see the equilibrium closed orbit for E = 10 MeV. Fig. 2.6 shows how the energy beam size decreases almost linearly as function of the energy for the longitudinal and radial plane of the distributions. The vertical plane appears to be more constant along the range.

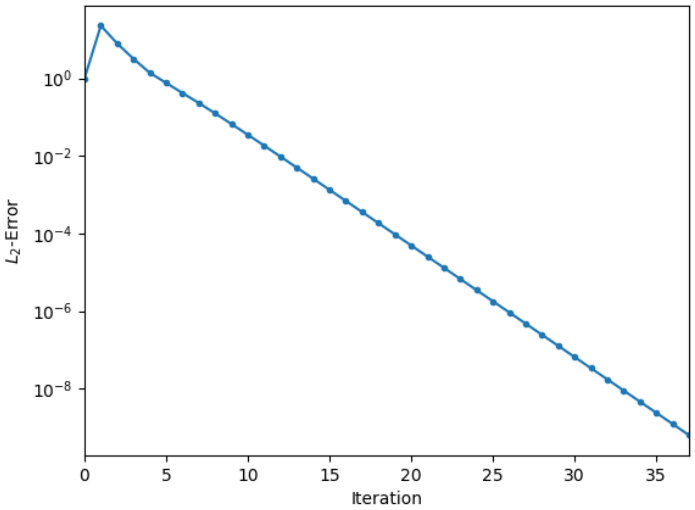

Figure 2.7: Convergence curve for a matched distribution.

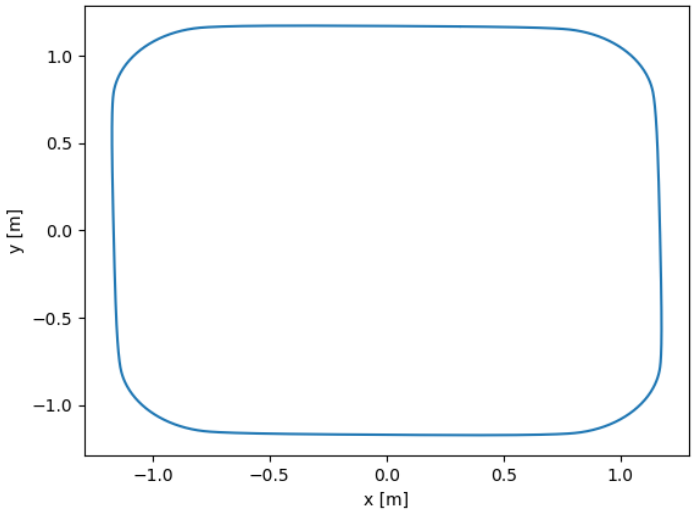

Figure 2.8: Closed orbit for Injector II for 10MeV.

2.2.2 Ring

Similar to the Injector II matched distributions were computed for the Ring. The same considerations regarding the numerical setup parameters for the simulation apply and most importantly $\Delta\phi$ affects the precision for high energetic ranges. Actually the effect of this parameter can be observed in Figure 2.5, where the margin of the Ring looks somehow distorted and not smoothly continuous.

Ring	
energy range [MeV]	72 - 590
energy stepsize [MeV]	2
injection angle [°]	110
angular stepsize [°]	0.25
convergece threshold	10^{-9}
max. # iterations	200
integration scheme	Runge-Kutta 4
emittance ε [π mm mrad]	2
current I [mA]	2.19
# macroparticles N	10000
dump frequency	10

Table 2.2: Numerical setup for the Ring.

The beam sizes for the energy range are shown in Fig. 2.9.

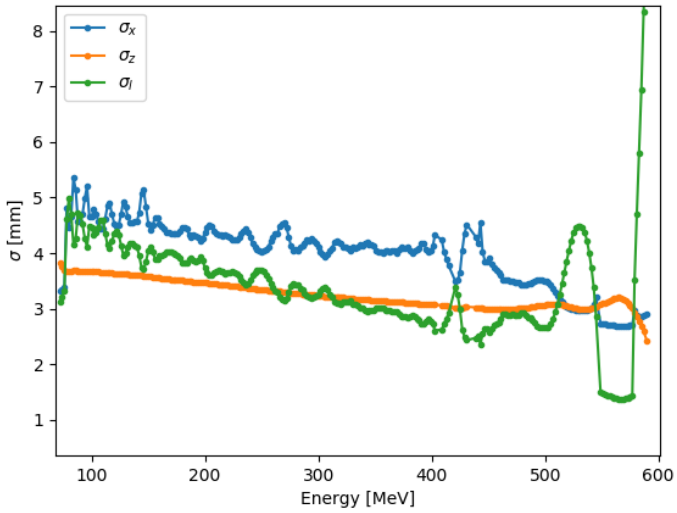

Figure 2.9: 1-σ beam size of the matched distributions at the Ring.

The results show good convergence over the full energy range, with some exceptions in the high energetic range(E > 400MeV). At first the radial and longitudinal beam sizes appear to be even smaller than the horizontal matched beam size. Considering just the range $E \in [75, 415]$, we observe the same behaviour as in the Injector, namely, the beam sizes decrease as a function of the energy. We observe an unexpected behaviour at the end of the energy range, since the longitudinal dimension of the beam appears to grow very fast. The reason for this is still unknown but there might be a bug in the reading of the field map for high energies. In Fig. 2.10 we can see the closed orbit for E = 92MeV. A convergence curve is not shown, since all the curves look qualitatively like Fig. 2.7.

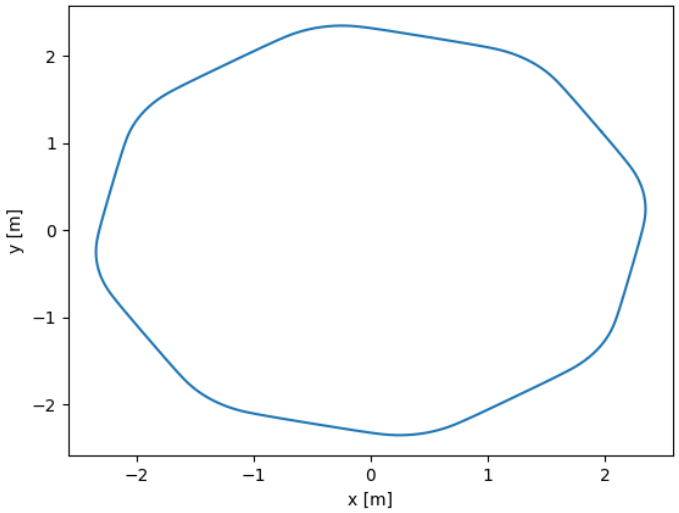

Figure 2.10: Equilibrium closed orbit in Ring for 92MeV.

2.3 OPAL tracking

In this section we present the results from the PIC tracking and compare it with the linear map tracking of the matched distributions, whose sizes are sketched in Figures 2.6 and 2.9. With the help from the covariance matrices, a bunch normally distributed was generated. The Gauss distribution might better describe the actual experimental setup, meaning that the bunches are most probably better approximated by a Gauss distribution in the cyclotron, than by a KV (hollow shell) or a waterbag distribution.

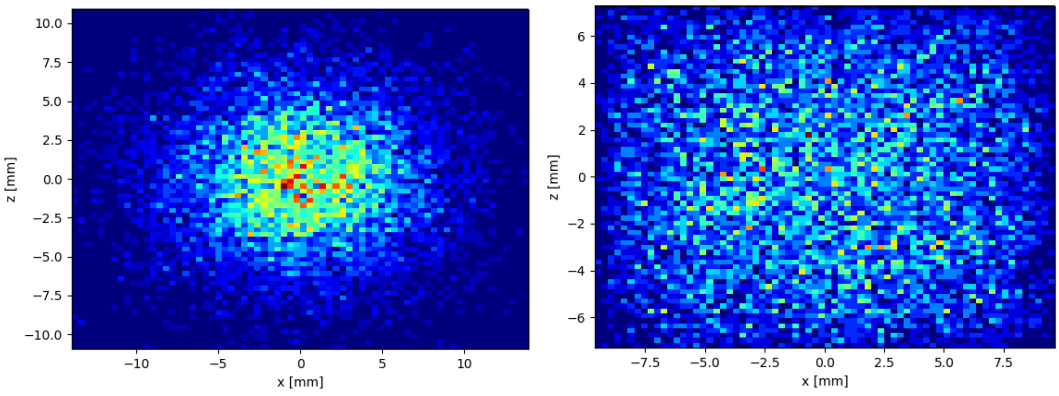

(a) Gauss distribution.

(b) Waterbag distribution.

Figure 2.11: Projection of the in OPAL generated distributions from matched covariance matrix for 78MeV in Ring (radial and vertical dimensions).

2.3.1 Injector II

First, we take a look at the beam envelope of a matched distribution. We choose E =43MeV. The following beam envelopes resulting from the PIC algorithm (blue) are plotted together with the ones resulting from the linear transfer matrices (orange). As briefly discussed above, the number of macro-particles N influences the generation of the bunch dimensions. The higher N, the better the initial bunch dimensions are generated. This discrepancy is later visible in every beam size plot. The dashed lines intersect in a point in the orbit where the distribution has approx. the same beam sizes as the initial distribution.

The results are shown in Figs. 2.12 - 2.14.

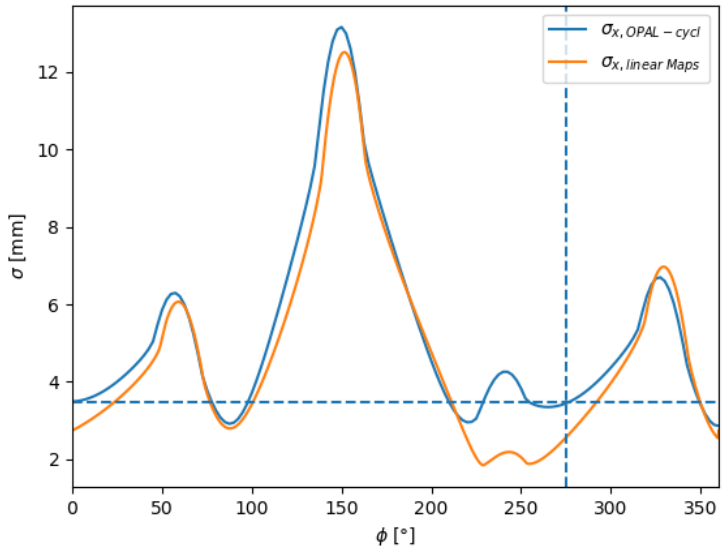

Figure 2.12: 1-σ beam envelope in Injector II for E = 43MeV. Radial dimension.

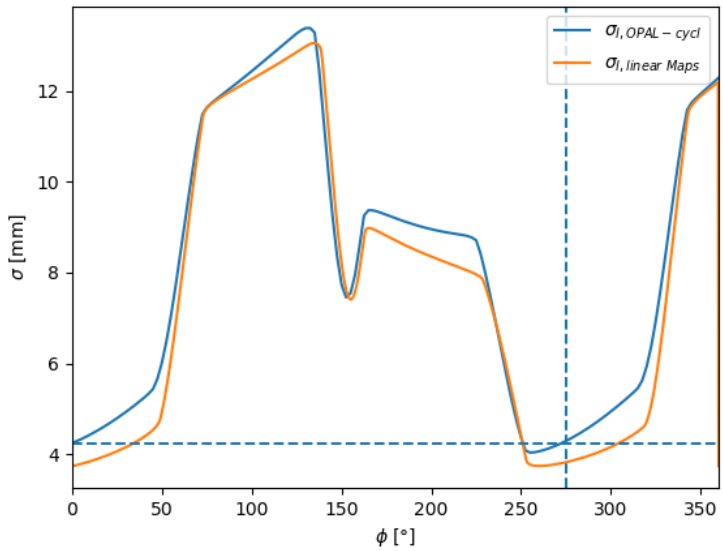

Figure 2.13: 1-σ beam envelope in Injector II for E = 43MeV. Longitudinal dimension.

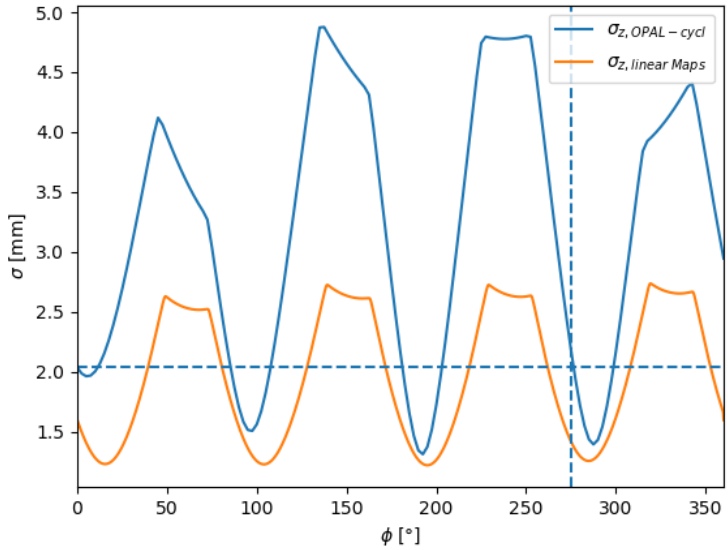

Figure 2.14: 1-σ beam envelope in Injector II for E = 43MeV. Vertical dimension.

The figures above show the evolution of the bunch in one turn. Although the initial beam envelopes are not strictly the same, we see that the linear transfer maps describe quite well the evolution of the system for the longitudinal and the radial direction. For the vertical direction, we recognize that the agreement is rather poor, nevertheless qualitatively there is a good picture. We can also immediatly recognize that the distribution is not matched to one turn (360°). The pointed vertical blue line intersects with the horizontal axis at $\phi = 275.5°$ and the horizontal one is a visual aid, that intersects the ordinate axis at the initial $1 - \sigma$ beam size.

Figure 2.15 shows the initial, final and our bunch at our candidate matching point:

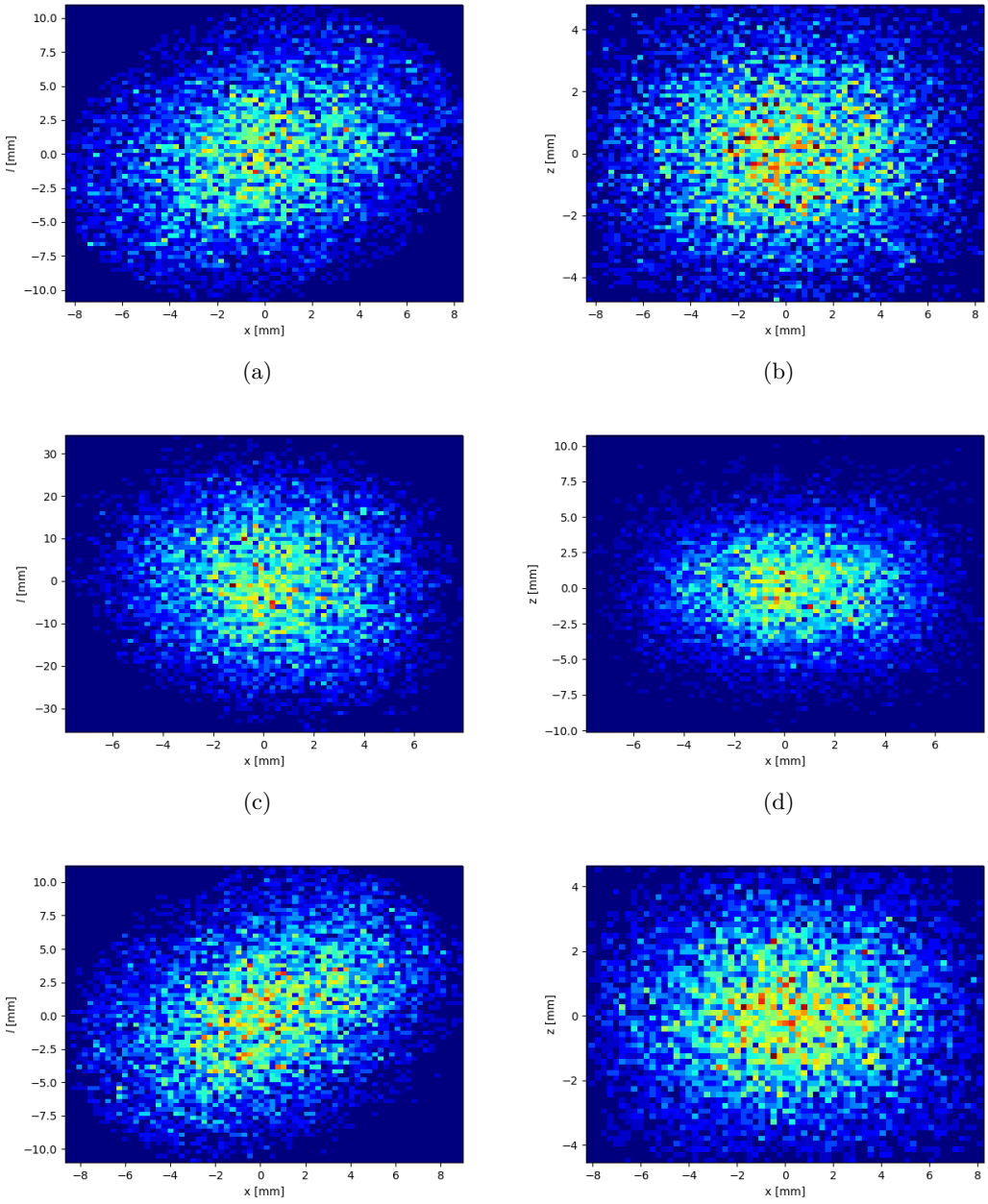

Figure 2.15: Initial (a,b), final (c,d), and matched (e,f) distribution (candidate) for E = 43MeV at Injector II.

At last, Figure 2.16 shows the difference between final and initial beam sizes ($\sigma(s = 360) - \sigma(s = 0)$). We can safely state that the distributions are not matched after one turn, especially

the longitudinal direction.

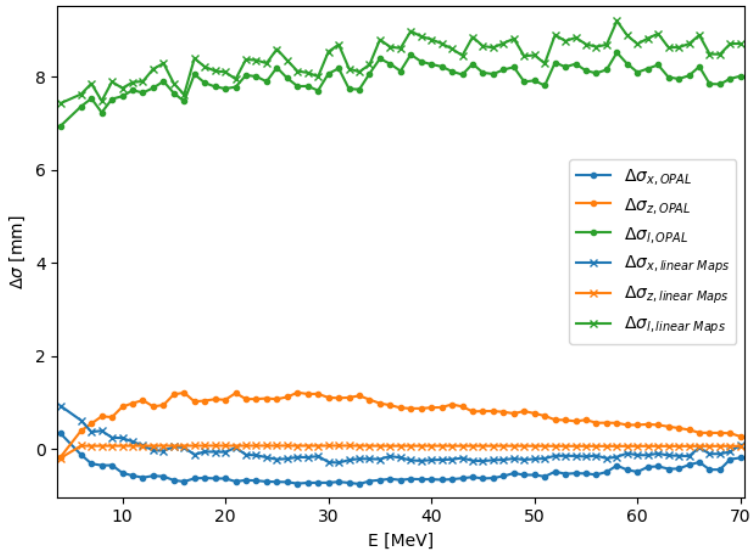

Figure 2.16: Difference between final and initial 1-σ beam size in Injector II.

2.3.2 Ring

For the Ring we present the same information as for the Injector II, but we take as an example the distribution found for E = 98MeV.

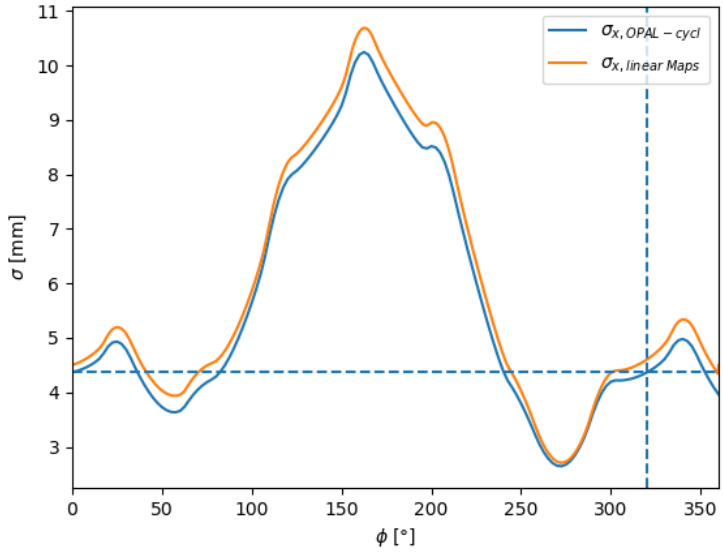

Figure 2.17: 1-σ beam envelope in Ring for E = 98MeV. Radial dimension.

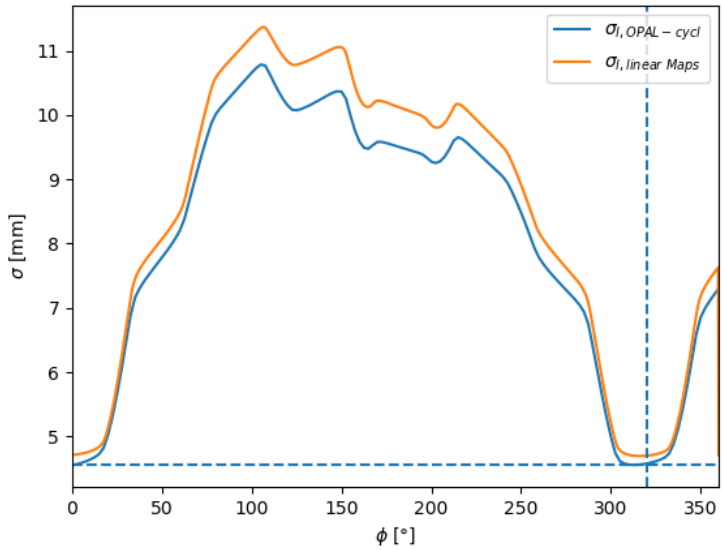

Figure 2.18: 1-σ beam envelope in Ring for E = 98MeV. Longitudinal dimension.

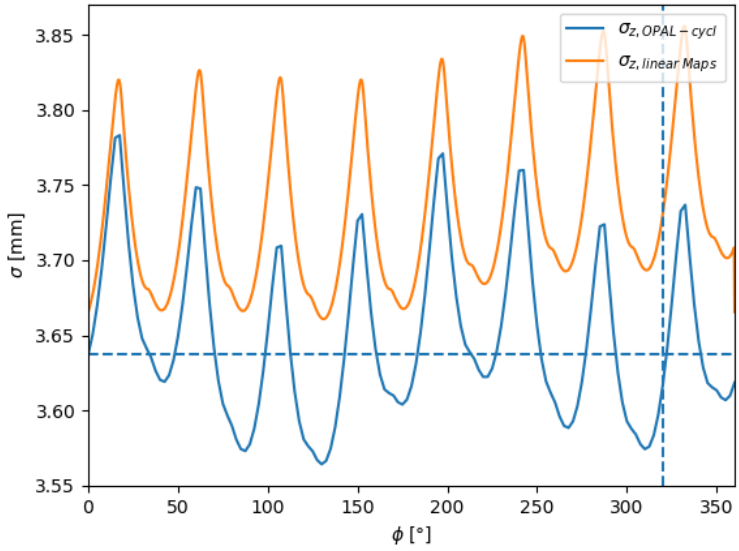

Figure 2.19: 1-σ beam envelope in Ring for E = 98MeV. Vertical dimension.

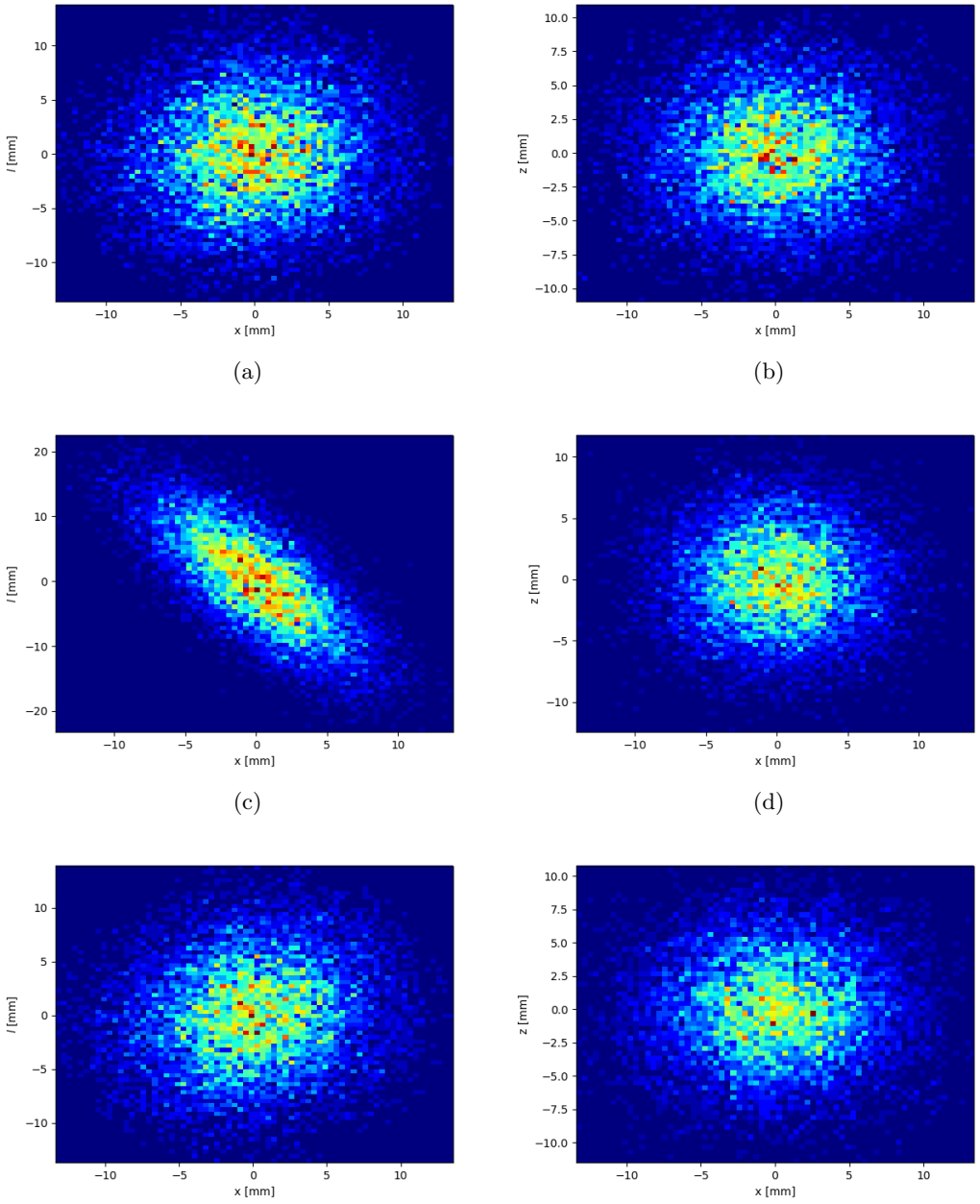

Figure 2.20: Initial (a,b), final (c,d), and matched (e,f) distribution (candidate) for E = 98MeV at Ring.

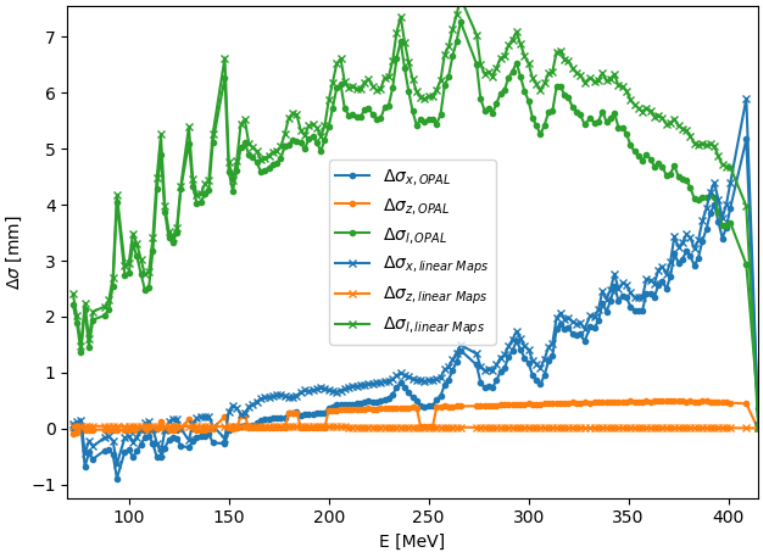

Figure 2.21: Difference between final and initial 1-σ beam size in Ring.

Figures 2.17, 2.18 and 2.19 show a good agreement between the linear maps and the OPAL tracking. We certainly see that the distributions are not matched to one turn and again, like in the Injector II. The vertical direction has a bigger discrepancy than the other two dimensions.

Figure 2.21 shows the difference from final and initial beam sizes in the energy range $E \in [72, 415]$ MeV. The presented range was chosen, because up until 409MeV the linear maps describe satisfactorily the results of the OPAL tracking, meaning that the orange curve from Figures 2.17 - 19 still describe qualitatively well the expected behaviour. The nature of the beam envelope look very similar for the energy range $E \in [78, 409]$ MeV, the first energy steps do behave differently, but both orange and blue curves agree. From now on, we leave aside the high energetic range (E > 409 MeV), because of the reason mentioned before.

Figures 2.15 and 2.20, give us an idea of how the distributions look like. The value where the pointed lines intersect in Figures 2.12-14 and 2.17-19 would certainly jump into the attention of the reader after long time investing in the task of carefully beholding such plots. This point becomes also especially interesting, if we contemplate Figures 2.15 and 2.20 (a,b,e,f) , where we can discover that even the correlation of the bunches is extremely similar.

Chapter 3

Analysis and Critical Assessment

3.1 Analysis of the data

In this chapter we discuss and assess the results presented in Chapter 2. The covariance matrix has 13 relevant parameters, which describe the matched distribution, but we mostly concentrate on describing the characteristics of the beam sizes, since key information can then be infered from them.

3.1.1 Initial beam sizes

The initial beam sizes of the computed matched distributions appear to decrease linearly as a function of the energy. Fitting a linear function of the form

$$\sigma_{init} = a \cdot E + \sigma_0 \tag{3.1}$$

to both data shown in Figures 2.6 and 2.9 led us to the following linear coefficients

	Injector II	Ring
$\sigma_{0,x}$[mm]	2.87 ± 0.01	4.91 ± 0.03
$\sigma_{0,z}$[mm]	1.71 ± 0.01	3.872 ± 0.003
$\sigma_{0,l}$[mm]	4.02 ± 0.02	4.87 ± 0.03
$a_x[\mu\text{m MeV}^{-1}]$	$-(2.2 \pm 0.2)$	$-(2.4 \pm 0.1)$
$a_z[\mu\text{m MeV}^{-1}]$	$-(1.8 \pm 0.3)$	$-(2.06 \pm 0.01)$
$a_l[\mu\text{m MeV}^{-1}]$	$-(7.4 \pm 0.2)$	$-(5.4 \pm 0.1)$

Table 3.1: Fit parameters for linear fit of the initial 1-σ bunch sizes.

The data was fitted with the help of Python 3, which uses the least squared method to fit the data to the given function. The uncertainties are given by the square root of the covariance matrix diagonal entries. Error bars are difficult to consider in this plot, since the numerical threshold used in OPAL is very low in comparison with the values and the initial uncertainty propagation from the quantities is not provided. Nonetheless we see that a linear fit is especially well suited for the beam sizes in Injector II. For the Ring we observe that for the low energy range the data is scattered more strongly for the longitudinal and radial dimensions. The vertical direction appears to be very well described by Eq. 3.1 with the coefficients in Table 3.1.

We see that for both machines the slopes $a_{x,z}$ appear to be in a 1-σ range similar. The longitudinal slope does not agree in this range. The parameter $\sigma_{0,x,z}$ appear to be approx. 2

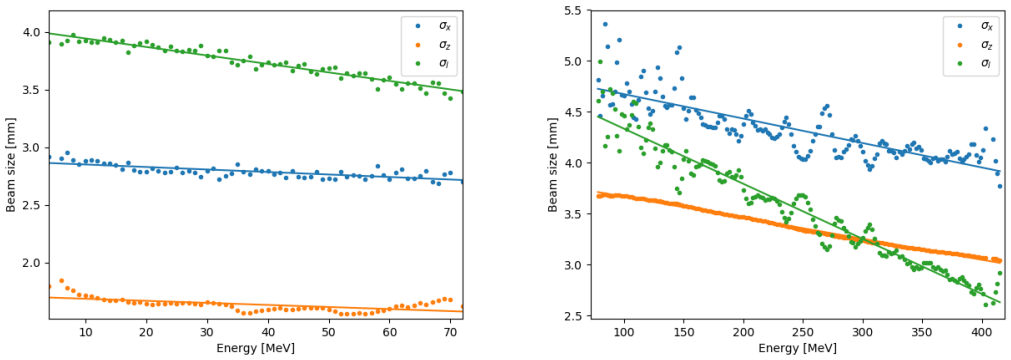

(a) Injector II (b) Ring

Figure 3.1: Linear fit of the initial 1-σ bunch sizes.

mm bigger in the Ring, than in the Injector II. The difference for the longitudinal direction is of (0.85 ± 0.04) mm.

3.1.2 Matching point

The theory presented in this thesis points to the expectation, that the matched distributions should be fairly identical after one turn in the machine, since we took in the computation the one turn transfer matrix. The results showed almost immediatly after first simulation attempts, that this is not the case.

The data still suggests, that there is a matching point, where the distribution looks very similar to the initial configuration. As we can see from the envelope plots presented above (Figs. 2.9 - 11 and Figs. 2.14 - 16), this point has a close relationship to the periodicity of the longitudinal dimension. If the longitudinal dimension can be described by a periodic function $\sigma_l(s+P) = \sigma_l(s)$, then, we come to the pragmatical hypothesis, that given the initial covariance matched distribution entries $\sigma_{ij}(s=0) = \sigma_{ij,0}$, it holds $\sigma_{ij,0} = \sigma_{ij}(s = nP), n \in \mathbb{N}_0$.

The first challenge to prove this observation, is the determination of the periodicity P, given that there is no theory available (to the knowledge of the author) dealing with this topic. Secondly as discussed before, the matched covariance matrix has 13 parameters, whose interpretation is difficult to summarize in one parameter without losing information. For this reason with the available data we exemplify to what extent does this hypothesis holds for the computed matched distributions in the machines.

To find the periodicity P, we take into account that at this point it should hold

$$\Delta\sigma = \sigma_{x,z,l}(s = P) - \sigma_{x,z,l}(s = 0) = 0. \tag{3.2}$$

Eq. 3.2 led to following Figures

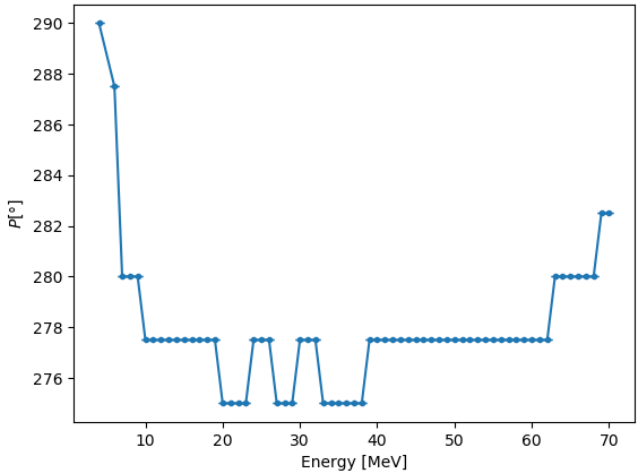

Figure 3.2: Injector II longitudinal periodicity as function of the energy.

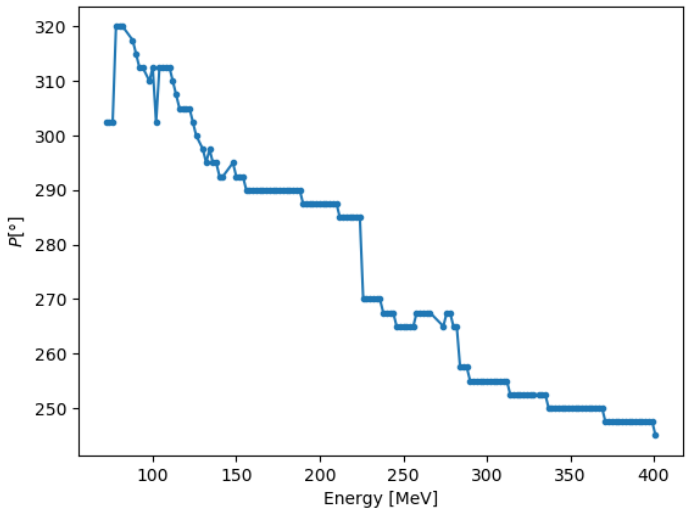

Figure 3.3: Ring longitudinal periodicity as function of the energy.

We observe that the longitudinal periodicity in the Injector II is mostly constant, whereas for the Ring, it decreases with increasing energy.

In Fig. 3.4 and 3.5 the difference between the initial 1-σ beam sizes and the beam sizes at the suggested matching point are shown (Eq. 3.2).

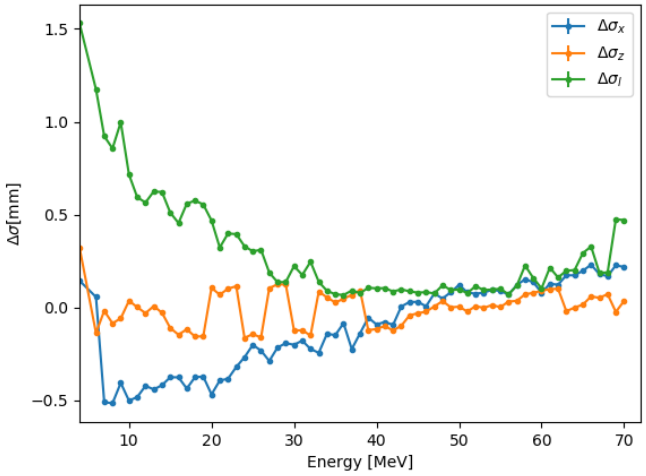

Figure 3.4: Injector II beam size increase at matching point.

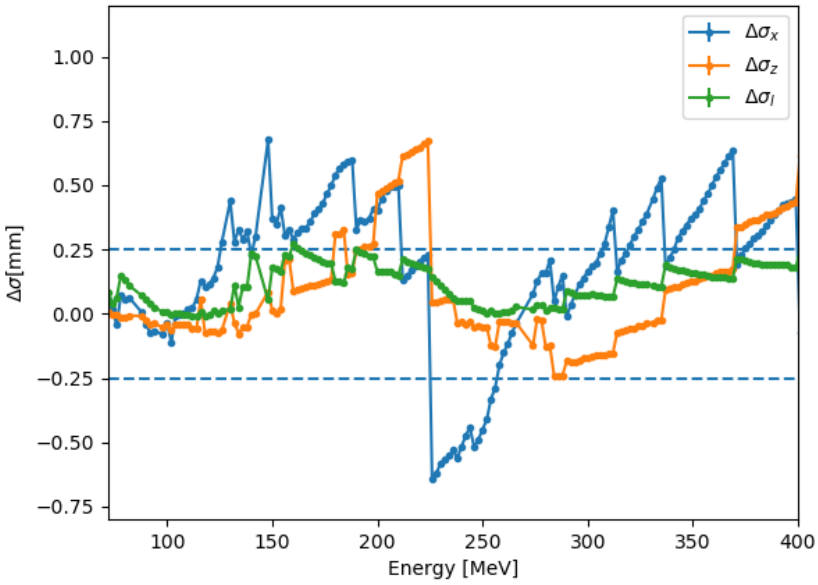

Figure 3.5: Ring beam size increase at matching point.

Figures 3.4 and 3.5 show ultimately to what extent are the distributions matched at this suggested point. If we compare Fig. 2.16, where the longitudinal beam size increase is approx. 8 mm with Fig. 3.4, we can see that at the matching point the distribution looks very similar to the initial one. Fig. 3.4 also has interesting features. As we can see, the longitudinal increase starts at approx. 1.5 mm, and then starts going to zero for increasing energy. The reason for this behaviour lies in the beam envelope. If we look for example at Fig. 2.12, the blue curve

intersects with the horizontal pointed line at the suggested matching point, this is not the case for the low energy range in the Injector II. The curve conserves the behaviour but does not come back to this point meaning that it is not stricktly periodic. For the high energy range we can appreciate that the beam size increase is rather low. This suggests that the existence of matched distributions is possible for this energy range in the Injector II. For the Ring we see a more dynamic picture. The increase is definitely lower than the one showed in Figure 2.21, where we mostly see an increase of the longitudinal dimension from 2 mm up to 7 mm. We also see, that the energy range from 72MeV to 126MeV and from 226MeV to 305MeV possess a very moderate beam size increase.

3.2 Conclusion and Outlook

3.2.1 Simulation results

We shall first start by discussing the quality of the data presented in Chapter 2. First of all, we recognize that the analysis of the machines was restricted by the integration step $\Delta\phi$, especially the high energetic range of the Ring. It is mandatory at some point to perform an uncertainty quantification, to better know how the numerical parameters influence the results. Not only this, but the uncertainties of magnetic field maps should be taken into consideration, since all the simulation relies on them. This is no easy task and goes beyond the scope of this thesis.

Secondly, it should certainly be accentuated the fact that the matched covariance matrices all across the Injector II and almost very few at the Ring (for the "well behaved" energy range), are numerically inconsistent. This means, that the computed matrices appear not to be strictly positive definite, in the sense that not all their eigenvalues are positive. This property is important for the computation of the correlation coefficients and a renormalization process was applied to overcome this issue. This lastly translates into the discrepancy between the initial beam sizes from the generated bunch and the ones computed by the matching algorithm, which adds up to the statistical difference, arising from the number of macro-particles in the bunch. The correlation coefficients are important for the distribution and for the simulation, since taking them into consideration improves the agreement of the beam envelope curves expected from the linear transfer maps and the ones delivered by the PIC algorithm. The reason for this is still unknown and is an indicator of a possible bug in OPAL.

Third, the poor description of the linear theory in the high energy range of the Ring can also rely on the fact, that the emittance we chose was too high. We can see that the beam envelope decreases as a function of the energy, mostly, because the space charge effect is inversely proportional to γ^3 (See e.g. Eq. 1.47). This implies, that the more energetic the bunch, the more stable it becomes, hence, lower emittance. Special attention should be given to this range, since at one later point the bunch is extracted, and stability is then very significant.

Lastly, the results delivered important information about the matched distributions and the influence of higher order space charge effects. We see that the beam envelopes can be very well modelled by the linear transfer maps, since the curves do not differ significantly from each other. If the bunch is indeed normally distributed, then, we can conclude from the data, that taking a linear space charge effect into consideration is enough to model the expected behaviour of the 1-σ beam envelope. This feature allows probably to further investigate higher currents, i.e., stronger space charge.

3.2.2 On the matched distributions

The information described in the analysis of the initial beam sizes of the matched distributions leads us to draw some conclusions. The initial beam sizes of the matched distributions computed on the Injector II do not change much in the energy range. This translates into the very small slopes presented in Table 3.1 and can suggest that taking the same matched distribution beam size for every energy configuration wouldn't make a big difference.

In the Ring, we notice a broad scattering in the initial beam sizes at low energy range, and we can even observe some sort of oscillation in the horizontal and longitudinal dimensions. This translates to the conclusion that a linear fit is rather poor but also in general it can somehow describe the energy dependency. Because the energy range is much wider than in the Injector II, we see that the beam sizes of the matched distribution changes more.

Another interesting feature would be investigating the moment characteristics (x', z', δ) of the matched beam, as well as all the correlations included in the covariance matrix. The moment deviations behave roughly speaking in the same way as the initial beam sizes but no quantitative analyses has yet been made.

Finally, it should be addressed the fact that the data does not match the theoretical expectation. As presented in the first Chapter there are various factors that could be responsible for this result. Although we can recognize that the simplified Hamiltonian does still contain a significant and relevant amount of information of the system, which can be corroborated by the PIC algorithm, we don't really know the implications that this linearisation has on the computation of the matched distribution.

Before commenting any further and taking aside the Hamiltonian the following passage in [7] appears to be very helpful:

> For most systems of interest we cannot write the transfer map in closed form; hence we usually resort to the use of approximations in the form of a Taylor map: "..." Hence the unavoidable truncation of the Taylor series (almost always) violates the symplectic condition. For some purpouses this (one hopes small) violation have a little effect; but for others, e.g.,long-term tracking using many iterations of the map, the consequences can be severe. Moreover, numerical studies have shown that these undesirable consequences often do not derive from the loss of high-order information in the truncated Taylor map but from the symplectic violation itself "..."

The first thing that came to mind, while trying to understand, why Eq. 1.60 was not fulfilled, was the following. As described before the implications of the approximations we made i.e. the truncation of the transfer map and the separation of the Hamiltonian (Eq. 1.48) were unknown. We can assert to state, that the truncation mainly impacts the simplectic condition described by Eq. 1.24, which was also a requirement for Eq. 1.61 to hold. This lastly influences the computation of the matched distribution with Eq. 1.62 and leading to the conclusion that it shouldn't hold since we don't have the prerequisite of a symplectic transfer map.

Nonetheless the algorithm did find matched distributions. The results presented in this thesis suggest some interesting information about the impact of the violation of the symplectic condition. The first trivial conclusion is that violating the symplectic condition, while computing a one turn matched distribution, does not deliver a one turn matched distribution. The data still suggests another conclusion about "moderately" violating the symplectic condition, if and only if, the hypothesis priorly presented is true; namely that violating "moderately" the symplectic condition, while computing a matched distribution leads to the displacement of the matching point and this matching point has a close relationship to the periodicity P of the longitudinal dimension. Whereas the later conclusion is valid should be more intensively investigated and

it is still inconclusive if there is still any hidden bug or bugs in the code, which led to these unexpected results. We certainly can benchmark these results for further improvement of the OPAL framework and study of matched distributions.

3.3 Acknowledgements

I would like to kindly thank Dr. Andreas Adelmann for giving me the opportunity to work at PSI in the LSM-AMAS group, in a topic, which I personally find quite interesting. I also want to thank and acknowledge Prof. Schöning for supporting my initiative to come to PSI. I especially thank don señor Matthias Frey, whose support was invaluable at critical points, where bugs and confusion appeared.
Last but not least, I want to thank my parents and my brother for their unconditional support during all my endeavours in life, and especially my mother, who always has helped me to broaden my horizon, regardless of the limitations and situations I'm in.

Bibliography

[1] Baumgarten, Christian. Transverse-longitudinal coupling by space charge in cyclotrons. Phys. Rev. ST Accel. Beams, 14:114201, 2011.

[2] Frey, Matthias. Semester thesis: Matched distributions in cyclotrons. 2015. http://amas.web.psi.ch/people/aadelmann/ETH-Accel-Lecture-1/projectscompleted/cse/frey-semester_thesis.pdf

[3] Adelmann, Andreas, et al. The OPAL Framework. 1. revision. June 2018. https://gitlab.psi.ch/OPAL/src/wikis/home.

[4] Hinterberger, Frank. Physik der Teilchenbeschleuniger und Ionenoptik. Springer Verlag. Zweite Auflage. 2008.

[5] Dragt, Alex. Lie Methods for Nonlinear Dynamics with Applications to Accelerator Physics. University of Maryland. 16 June 2018. https://www.physics.umd.edu/dsat/.

[6] Wolski, Andrej. Lecture 3: The accelerator hamiltonian in a curved coordinate system. University of Liverpool and the Cockcroft Institute, Daresbury, UK. 2012. http://pcwww.liv.ac.uk/ awolski/.

[7] Abell, Dan. Fast symplectic map tracking for the CERN Large Hadron Collider. Phys. Rev. ST Accel. and Beams. Vol 6, 064001, 23 June2013.

[8] Hockney, R. and Eastwood, J. Computer Simulation Using Particles. Taylor & Francis Group. 1998.

[9] Yang, J.J., et al. Beam dynamics in high intensity cyclotrons including neighboring bunch effects: Model, implementation and application. Phys. Rev. ST - Accelerators and Beams 13, 064201, 2010.

[10] A. Kolano; A. Adelmann, et al. Intensity limits of the PSI Injector II cyclotron. Nuclear Instruments & Methods in Physics Research, A. 2017.

[11] Wolski, Andrzej. Alternative approach to coupled linear optics. Lawrence Berkeley National Laboratory, 2005.

[12] Frey, Matthias. Master thesis. Matched distributions in cyclotrons with higher order moments of the charge distribution. 28 September 2015. http://amas.web.psi.ch/people/aadelmann/ETH-Accel-Lecture-1/projectscompleted/cse/MScThesis_Frey.pdf

[13] Bartelmann, Matthias. Theoretische Physik I: Punktmechanik und mathematische Methoden. Vorlesung Skript, WS 2015/2016.

[14] Bartelmann, Matthias. Theoretische Physik II: Analytische Mechanik und Grundlagen der Thermodynamik. Vorlesung Skript, SS 2016.

[15] Ewerz, Carlo. Theoretische Physik III: Klassiche Elektrodynamik. Vorlesung Skript, WS 2016/2017.

[16] Berz, Martin. Modern Map Methods in Particle Beam Physics. Academic Press. 1999.

[17] Paul Scherrer Institute. The PSI Accelerator online-Wiki. http://acceleratorwiki.psi.ch/wiki/Hauptseite.

[18] Coordinate System. https://cds.cern.ch/record/2206741/plots.

[19] Cyclotron sketch. https://sites.google.com/site/puenggphysics/home/unit-iii/cyclotron.

[20] PSI Ring Cyclotron. http://acceleratorwiki.psi.ch/wiki/Einfürung_Hochstromprotonen beschleuniger_(Anfänger).

[21] HIPA Facility sketch. http://acceleratorwiki.psi.ch/wiki/Datei:HIPA3DUbersicht.jpg.

[22] Injector II sketch. http://acceleratorwiki.psi.ch/wiki/Einfürung_Hochstromprotonenbe schleuniger_(Anfänger) #Injektor-2.

[23] PSI Ring cyclotron sketch. http://acceleratorwiki.psi.ch/wiki/Datei:590MeVRingQuerschnitt Grundriss.PNG.

Erklärung

Ich versichere, dass ich diese Arbeit selbstständig verfasst und keine anderen als die angegebenen Quellen und Hilfsmittel benutzt habe.

Heidelberg, den 31 Oktober, 2018.